



# A Spatial Model Comparing Above- and Belowground Blue Carbon Stocks in Southwest Florida Mangroves and Salt Marshes

Kara R. Radabaugh<sup>1</sup> · Ryan P. Moyer<sup>1,2</sup> · Amanda R. Chappel<sup>1,3,4</sup> · Joshua L. Breithaupt<sup>1,5</sup> · David Lagomasino<sup>6</sup> · Emma E. Dontis<sup>1,4,7</sup> · Christine E. Russo<sup>1,3,8</sup> · Brad E. Rosenheim<sup>4</sup> · Lisa G. Chambers<sup>9</sup> · Elitsa I. Peneva-Reed<sup>10,11</sup> · Joseph M. Smoak<sup>4</sup>

Received: 12 October 2022 / Revised: 4 March 2023 / Accepted: 8 May 2023  
© The Author(s), under exclusive licence to Coastal and Estuarine Research Federation 2023

## Abstract

Blue carbon ecosystems such as mangroves and salt marshes store large amounts of carbon (C) in the form of plant biomass and soils that are often rich in organic matter. These C stocks have a high degree of spatial variability within and among coastal wetland ecosystem types, but quantifying location-specific C stocks is both labor intensive and time-consuming. Above- and belowground C stock data were compiled from field efforts in Southwest Florida and from published georeferenced C data. These data were used in conjunction with ecosystem maps, remote-sensing parameters, and existing vegetation models to create 30-m resolution spatial models quantifying aboveground C stocks and belowground C stocks up to 1-m depth in mangroves and salt marshes along 360 km of coast in Southwest Florida (Tampa Bay to the Everglades). Based on modeling results, mangroves and salt marshes in Southwest Florida store an average of  $393.9 \pm 107.1$  and  $286.7 \pm 71.9$  Mg C ha<sup>-1</sup>, respectively, in above- and belowground C stocks. Soil C density and belowground C stocks increased at lower latitudes within the study region. Total C stocks in mangroves increased from  $265.1 \pm 43.2$  Mg ha<sup>-1</sup> in Tampa Bay and Sarasota Bay to  $409 \pm 104.4$  Mg ha<sup>-1</sup> in the Everglades. Substrate stability and C stocks are susceptible to impacts from climate change, sea-level rise, hydrologic changes, and episodic disturbances such as tropical cyclones. The long-term storage of C in these ecosystem types depends on ecosystem stability in the face of these stressors.

**Keywords** Organic carbon · Remote sensing · Coastal wetland · Random forest · Biomass

Communicated by Just Cebrian

✉ Kara R. Radabaugh  
kara.radabaugh@myfwc.com

- <sup>1</sup> Florida Fish and Wildlife Conservation Commission, Fish and Wildlife Research Institute, Saint Petersburg, FL, USA
- <sup>2</sup> TerraCarbon LLC, Saint Petersburg, FL, USA
- <sup>3</sup> University of Florida, Gainesville, FL, USA
- <sup>4</sup> University of South Florida, Tampa, FL, USA
- <sup>5</sup> Florida State University Coastal & Marine Laboratory, St. Teresa, FL, USA
- <sup>6</sup> Integrated Coastal Programs, East Carolina University, Wanchese, NC, USA
- <sup>7</sup> Pinellas County, Clearwater, FL, USA
- <sup>8</sup> Manatee County, Bradenton, FL, USA
- <sup>9</sup> University of Central Florida, Orlando, FL, USA
- <sup>10</sup> United States Geological Survey, Reston, VA, USA
- <sup>11</sup> The World Bank, Washington, DC, USA

## Introduction

Coastal wetlands are important to global carbon (C) cycles and store a disproportionately large amount of organic carbon (OC) per hectare compared to terrestrial ecosystems (Donato et al. 2011; Kauffman et al. 2011; Alongi 2014, 2020). Coastal wetlands are known as blue C ecosystems due to their ability to capture atmospheric carbon dioxide through photosynthesis, convert it to OC in vegetative biomass, and sequester it long-term in soil. The OC in blue C ecosystems is primarily stored belowground in live and dead roots and in the soil itself. Decomposition is slow within the anoxic and water-saturated soil, enabling the preservation of OC for centuries to millennia (Orson et al. 1987; Donato et al. 2011; Alongi 2020; Feagin et al. 2020). Coastal wetlands can form peat deposits (soils with > 20% organic matter), which are formed through the accumulation of roots with additional organic contributions from aboveground biomass and allochthonous inputs including

seagrass and estuarine particulate organic matter (Middleton and McKee 2001; Bouillon et al. 2003; Chmura et al. 2003; Maher et al. 2013; Alongi 2014, 2020).

Globally, mean above- and belowground C stocks are 739 Mg C ha<sup>-1</sup> in mangroves and 334 Mg C ha<sup>-1</sup> in salt marshes (Alongi 2020). However, these estimates vary widely with latitude, climate, vegetation type, soil biogeochemistry, and local geomorphology (Kauffman et al. 2011; Sanders et al. 2016; Ewers Lewis et al. 2018). On a global scale, both above- and belowground C stocks in mangroves are generally greater at lower latitudes, but there can be considerable local variability (Alongi 2014; Hutchison et al. 2014; Sanders et al. 2016; Simard et al. 2019a, b). This trend is largely driven by climate. Mangroves can grow taller and have greater biomass near the equator due to the warm temperatures, high precipitation, and reduced cyclone frequency (Simard et al. 2019a). However, tree height can be quite variable on a local scale depending on distance from the coast, inundation frequency, salinity, and geomorphic characteristics (Lara and Cohen 2006; Simard et al. 2006). Belowground C stocks also tend to be higher at lower latitudes as the increased precipitation can increase water logging, thus decreasing rates of decomposition in the saturated soil (Alongi 2013; Sanders et al. 2016). On a smaller scale, belowground C stocks are also influenced by allochthonous input, nutrient enrichment, vegetation assemblages, root biomass, wetland elevation, tidal amplitude, and local geomorphology (Kauffman et al. 2011; Sanders et al. 2016; Gress et al. 2017; Ouyang et al. 2017; Rovai et al. 2018; Simard et al. 2019a; Worthington et al. 2020).

Location-specific quantification of above- and belowground C stocks has been the primary focus of many blue C studies and is critical to accurately understanding and quantifying coastal biogeochemical cycles (e.g., Bouillon et al. 2008; Alongi 2012, 2014; Bauer et al. 2013). However, the expensive and labor-intensive nature of C stock quantification has led to several efforts to model coastal C stocks at both regional and global scales to improve C inventories and to explore the underlying drivers (e.g., Gress et al. 2017; Byrd et al. 2018; Sanderman et al. 2018; Campbell et al. 2022). Global models of soil C in mangrove forests have generally relied on latitude and climatic variables such as precipitation and temperature to predict much of the variability found in C stocks (Hutchison et al. 2014; Jardine and Siikamäki 2014; Rovai et al. 2018). Remote-sensing predictors of more localized factors, such as total suspended sediment, canopy height, and spectral data from Landsat imagery, have sometimes been included for additional explanatory power (Sanderman et al. 2018; Simard et al. 2019a, b; Campbell et al. 2022).

Aboveground C stocks in coastal wetlands are typically smaller compared to belowground stocks (Alongi 2020; Kauffman et al. 2020). Aboveground plant biomass

comprises only 1% of total C stocks found in salt marshes and 15% in mangroves, with the remaining C stocks found belowground as roots and in soil (Alongi 2020). The aboveground biomass of mangroves and other forests has been modeled with the use of airborne or satellite-based lidar and radar, which makes use of tree height as a predictor of forest biomass (Simard et al. 2006, 2019a; Lu et al. 2016; Fatoyinbo et al. 2018; Stovall et al. 2021). These biomass estimates can then be converted into aboveground C stocks based on the average C content of the vegetation (Howard et al. 2014; Stringer et al. 2015). Modeling aboveground biomass or C content in salt marshes is more challenging than in mangrove forests due to the broad variety of species found in salt marshes, including mixes of herbaceous and woody vegetation. It is also challenging to use remote sensing to measure vegetation height or elevation in salt marshes as measurements on the top of the plants are more accurate than ground measurements due to the inability of lidar to penetrate dense graminoid vegetation (Hladik and Alber 2012; Medeiros et al. 2015; Enwright et al. 2017; Thomas et al. 2019).

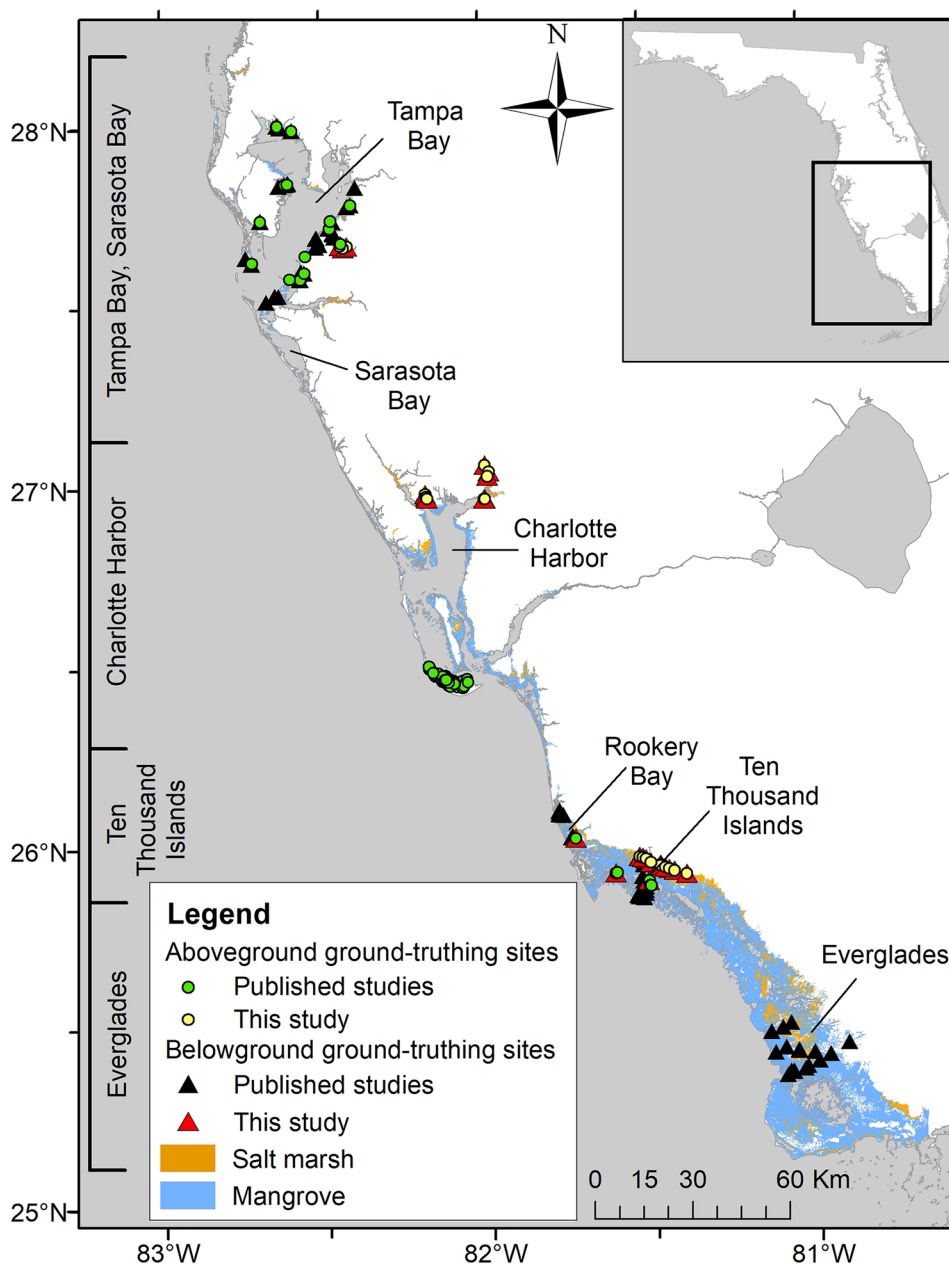
Global C stock averages and C models for mangroves are often dominated by data acquired in low-latitude Indo-Pacific mangrove forests (Alongi 2012, 2014). The nature of global models does not allow for the incorporation of the wide ecosystem variability found across the climatic gradient in Florida. Approximately 246,000 ha of mangroves and 151,000 ha of salt marshes remain in Florida, with Southwest Florida containing nearly 58% of the state's remaining coastal wetlands (SFWMD 2018; SFWMD 2019). Mangroves and salt marshes intermix in Southwest Florida; thus, a complete understanding of C stocks requires region-specific quantification and high-resolution consideration of both ecosystems and the transition zones between them. This study combined *in situ* field efforts, data from previously published studies, and remote-sensing data to quantify regional OC storage and model spatial variability of above- and belowground OC stocks at a 30-m resolution in mangroves and salt marshes in Southwest Florida. The objectives of this study were to model above- and belowground OC stocks across Southwest Florida coastal wetlands in order to examine large- and small-scale spatial trends of regional C stocks within the context of long-term ecosystem stability.

## Methods

### Study Region

This study focused on the coast of Southwest Florida, from Tampa Bay through the Everglades (Fig. 1). The region spans a climatic gradient, from a humid subtropical climate in the north to a tropical savanna climate in the south (Kottek

**Fig. 1** Coastal wetland extent and ground-truthing data (including both novel data collected for this study and published datasets) in Southwest Florida. Ranges of four regions used for data comparison are shown at the left of the figure. Salt marsh and mangrove extent obtained from water management district land use/land cover maps (SFWMD 2018; SWFWMD 2019)



et al. 2006). Salt marsh and mangroves are found throughout the region and have a year-round growing season, with increased rates of growth in the summer rainy season (Lugo and Snedaker 1974). Mangrove species include *Rhizophora mangle* (red mangrove), *Avicennia germinans* (black mangrove), and *Laguncularia racemosa* (white mangrove). The mangrove associate *Conocarpus erectus* (buttonwood) is also common. Dominant salt marsh species include *Juncus roemerianus* (black needlerush) and *Spartina alterniflora* (smooth cordgrass), which are intermixed with other graminoids (e.g., *Spartina* spp., *Panicum* spp., *Sporobolus virginicus*, and *Muhlenbergia capillaris*), succulents (e.g., *Batis maritima*, *Sesuvium portulacastrum*, *Blutaparon*

*vermiculare*, and *Salicornia* spp.), ferns (*Acrostichum dan-aefolium*), and small trees (e.g., *Baccharis halimifolia* and *Iva frutescens*). Mangroves are typically found closest to the shoreline, with salt marshes often present farther inland (Fig. 1).

### Field Data Collection

A total of 25 10×10-m plots were sampled in mangroves and salt marshes across Southwest Florida (locations listed in Tables S1 and S2 in Electronic Supplementary Materials). A real-time kinematic global-positioning system (RTK-GPS) Champion WR1 receiver (Champion Instruments, Norcross,

GA) and coupled HC1 data collector running Carlson SurvCE v 5.07 (Carlson Software Inc., Maysville, KY) were used to measure elevation and location at the corners of each 10×10-m plot. Real-time base-station corrections were made via direct cellular data connection to the Florida Permanent Reference Network (FPRN) maintained by the Florida Department of Transportation (<https://www.fdot.gov/geospatial/fprn.shtm>).

Woody vegetation was classified based on height and diameter at breast height (130 cm above the ground,  $d_{130}$ ). Vegetation categories included trees ( $d_{130} > 5$  cm), saplings ( $d_{130} < 5$  cm and height  $> 130$  cm), shrubs (height 30–130 cm), and seedlings (height  $< 30$  cm). The  $d_{130}$ , species, and status (live, recently dead with minimal decay, or decaying) were recorded for all trees within the 10×10-m plot. Saplings, shrubs, and seedlings were measured in a 5×5-m subplot that was established in the corner most representative of woody vegetation within the plot. The  $d_{130}$ , species, and status were recorded for each sapling. Species, diameter at 30 cm above the ground ( $d_{30}$ ), canopy dimensions (length, width, and depth), and total height of up to 25 shrubs were recorded, and the total number of shrubs was counted. The total number of mangrove seedlings was recorded along with the heights of up to 30 seedlings, and percent species composition of all seedlings was visually estimated.

In plots with herbaceous vegetation, 30×30-cm subplots were created in each corner of the 10×10-m plots. Heights of up to 25 stems of each species within each subplot were then recorded, along with the total number of stems and the ratio of live:dead stems. For herbaceous species and seedlings without published allometric equations relating plant height to biomass (see Tables S3 and S4 in Electronic Supplementary Materials), approximately 50 stems of varying height of each species were harvested for the creation of new allometric equations. Collected plants were refrigerated upon return from the field.

Two cores were retrieved per 10×10-m plot, collected in opposite corners of the plots. A D-type half-cylinder “Russian” peat corer (Eijkelkamp USA, Morrisville, NC) was used to remove an uncompacted soil core (5-cm diameter) to a depth of up to 50 cm. If surficial peat extended to a depth greater than 50 cm, a second core was removed adjacent to the original core up to a depth of 100 cm. Cores were photographed and stored in a half-cut polyvinylchloride (PVC) pipe wrapped in PVC food-service cling wrap. Cores were refrigerated upon return from the field to prevent desiccation or oxidation prior to analysis.

## Laboratory Methods

Plants collected in the field (salt marsh plants and some woody seedlings) were measured and dried within a few

days of collection. Stem lengths were recorded to the nearest 0.5 cm, then dried in an Isotemp 500 series or Heratherm OGS60 drying oven (Thermo Fisher Scientific, Waltham, MA, USA) at 60 °C until mass stabilized, usually around 72 h. Dry biomass was measured using an Ohaus Adventurer analytical balance (Ohaus Corporation, Parsippany, NJ, USA). Allometric equations were generated following the methods in Radabaugh et al. (2017) and are listed in Table S4 of Electronic Supplementary Materials.

Sediment cores were analyzed following a staged loss-on-ignition (LOI) combustion protocol to determine organic matter content of the soil and associated fine roots (the OC in roots and soil is collectively referred to as belowground C in this study). The LOI protocol used methods originally described by Ball (1964) and Dean (1974) with modifications suggested by Craft et al. (1991) and use of temperatures and ignition times recommended by Bengtsson and Enell (1986) and Plater et al. (2015). Each core was sectioned into 1-cm intervals, and a cylindrical aliquot of known volume (1.131 cm<sup>3</sup>) was removed from each interval and placed into a pre-weighed crucible. The soil aliquots were then dried in a Thermolyne furnace (Thermo Scientific, Waltham, MA) at 105 °C for 24 h, and their dry weights were recorded using a Mettler Toledo NewClassic MF balance (Mettler Toledo, Columbus, OH, USA). Dry bulk density was calculated as dry mass divided by initial aliquot volume. The samples underwent combustion at 550 °C for 3 h to remove organic matter. The percent organic matter that was lost on ignition (%LOI) was calculated as a function of dry mass ( $m_{dry}$ , g) and mass after combustion at 550 °C ( $m_{550}$ , g):

$$\%LOI = \left( \frac{m_{dry} - m_{550}}{m_{dry}} \right) \times 100 \quad (1)$$

Location and ecosystem-specific conversion equations were used to derive %OC from %LOI. Equation 2 (derived from Tampa Bay mangrove samples; Radabaugh et al. 2018) was used for Tampa Bay and Charlotte Harbor mangroves. Equation 3 was used for Tampa Bay and Charlotte Harbor marshes and salt flats (equation derived from Tampa Bay salt marsh samples; Radabaugh et al. 2018). Equation 4 was used for all other samples; this equation is a statewide, Florida-specific equation developed from mangrove soils with a wide variety of organic content (see Figure S1 and Table S5 in Electronic Supplementary Materials for further details).

$$\%OC = 0.42374 * \%LOI \quad (2)$$

$$\%OC = 0.50396 * \%LOI \quad (3)$$

$$\%OC = 0.001 * \%LOI^2 + 0.371 * \%LOI + 0.460 \quad (4)$$

## Compilation of Published Datasets and Calculations

Aboveground data collected during field efforts in this study were combined with aboveground data from Radabaugh et al. (2018, 2020) and Peneva-Reed and Zhu (2019; see Table S1 in Electronic Supplementary Materials). The aboveground dataset included C stocks from 86 locations (Fig. 1). Field work for these 86 locations was conducted between 2015 and 2020. Hurricane Irma made landfall in Southwest Florida in September of 2017 and caused extensive damage to mangrove forests (McCarthy et al. 2020; Osland et al. 2020; Radabaugh et al. 2020; Lagomasino et al. 2021). Aboveground data were either collected before Hurricane Irma, in locations not significantly impacted by Irma, or in the case of Radabaugh et al. (2020), data collected post-storm on recently felled trees were used to calculate pre-storm forest biomass.

Novel and previously published allometric equations (listed in Tables S3 and S4 in the Electronic Supplementary Materials) were used to calculate the aboveground biomass of woody and herbaceous vegetation. Biomass of woody vegetation was converted to C stock using a C conversion factor (proportion of C in dry biomass) of 0.44, based on data from Florida mangroves (Ewe et al. 2006; Bouillon et al. 2008). In locations where data were collected after Hurricane Irma, aboveground biomass of recently dead trees was calculated the same as live trees in order to calculate biomass prior to the hurricane. Aboveground biomass of decaying trees was calculated by using live tree equations and then subtracting 30% of biomass to account for loss of tree limbs and canopy (Howard et al. 2014). A carbon conversion factor of 0.5 was used for standing dead trees (Kauffman and Donato 2012; Howard et al. 2014). Carbon conversion factors for live herbaceous vegetation were obtained from Radabaugh et al. (2017), using species-specific C conversion factors when available or a factor of 0.411 for all other species. A C conversion factor of 0.45 was used for dead herbaceous vegetation (Howard et al. 2014). All aboveground C components were summed per plot area and used to calculate aboveground carbon stock ( $\text{Mg ha}^{-1}$ ). All above- and belowground ground-truthing data were classified by ecosystem type as either (1) mangroves or (2) salt marsh/other ecosystems (including sparsely vegetated salt flats or salt marshes mixed with woody vegetation such as *C. erectus*, *B. halimifolia*, or occasional small mangroves).

Additional belowground OC stock data (including belowground vegetation and soils) were compiled from the Coastal Carbon Atlas (Coastal Carbon Research Coordination Network, CCRCN; <https://ccrcn.shinyapps.io/CoastalCarbonAtlas/>) and other available data sources (see Table S2 in Electronic Supplementary Materials). Belowground C data sources included Cahoon and Lynch (1997), Chen and Twilley (1999), Breithaupt et al. (2014, 2017, 2020), Marchio et al. (2016), Gerlach et al. (2017),

Osland et al. (2012, 2016), and Radabaugh et al. (2018, 2020, 2021). If data from the CCRCN included %OC, the published %OC values were used as provided. If only %LOI was provided, %LOI was converted using Eqs. 2 and 3 for Tampa Bay and Charlotte Harbor mangroves and salt marshes, respectively. Equation 4 was used for all other samples south of Charlotte Harbor.

Years of core collection, from the CCRCN dataset and cores collected for this study, ranged from 1995 to 2020, with the majority of cores collected after 2010. Core data were not included from areas heavily impacted by Hurricane Irma. Cores from created wetlands were not included in the dataset. Only data from the top 1 m of soil were used for the model. The decision to limit the model to 1-m depth was based on recommendations of standard blue C procedures (Howard et al. 2014) and the paucity of deep sediment data (only 6 of the 421 cores in the dataset used to build the model extended to depths beyond 1 m). Multiple datasets from cores extending to 1 m depth were available for Tampa Bay and Sarasota Bay, Charlotte Harbor, and the Ten Thousand Islands. Cores from the Everglades reached a maximum of 60-cm depth.

## Model Methods

Machine-learning models were created in R version 3.6.2 (R Core Team 2019) using the *randomForest* package (Liaw and Wiener 2002). The random forest approach enables modeling of non-linear relationships between predictors and C stocks (Hengl et al. 2017). Two-thirds of the datapoints in each dataset were randomly assigned to a calibration dataset and one third retained for cross-validation and to test for overfitting. Separate models were created for aboveground OC stocks ( $\text{Mg ha}^{-1}$ ) and depth-specific soil OC density ( $\text{kg C m}^{-3}$ ). The belowground model predicted soil C density rather than total C stocks to model changes in C density with depth and because the maximum depth of cores within the dataset varied. Random forest models were created using spatially explicit predictor variables derived from remote-sensing data. These predictors, which were all obtained as rasters with a 30-m spatial resolution, included the following:

- Maximum canopy height of mangroves in 2000 (nominal year) from Simard et al. (2019b)
- Percentage of tree canopy cover in 2000 from Hansen et al. (2013)
- Landsat 8 data (Bands 1–8 and 10–11) from February 2015, obtained from USGS Global Visualization Viewer (GloVis; <https://glovis.usgs.gov/>)
- Normalized difference vegetation index (NDVI), as calculated from Landsat 8 bands 4 and 5 from February 2015, obtained from USGS Global Visualization Viewer (GloVis; <https://glovis.usgs.gov/>)

- arc-second DEM (USGS 2019), obtained from <https://apps.nationalmap.gov/downloader/#productGroupSearch>

Values for the predictors listed above were extracted using the package *raster* (Hijmans 2020) using the latitude and longitude for the location of each core and for the center of each vegetation plot. The Simard et al. (2019b) mangrove height data were limited to areas covered by mangroves; all locations lacking mangrove height data were assigned a value of zero. The number of predictors for the final models was selected based on the minimum error using the cross-validation procedure in the *randomForest* package.

A grid of points spaced at 30×30-m intervals was created in QGIS (version 3.14.15; QGIS Development Team 2020) in mangrove or salt marsh as mapped in Water Management District Land Use/Land Cover maps, which were created based on imagery collected in 2014–2017 (SFWMD 2018; SFWMD 2019). Carbon density in soils at depths of 0–1, 15–16, 30–31, 50–51, and 100–101 cm and aboveground C stocks were then predicted using the two random forest models based upon predictor data extracted for each of the gridded points. Belowground C stocks were integrated as a function of C density across depths 0–100 cm using the trapezoidal rule (Hengl et al. 2017). Above- and belowground C stocks ( $\text{Mg ha}^{-1}$ ) were plotted as rasters across Southwest Florida. An online version of this model was created using ArcGIS Experience Builder (ESRI, Redlands, CA, USA).

Statistical analyses were completed in R version 3.6.2 (R Core Team 2019). Significance was assessed at an alpha of 0.05. Data were examined for normality using Shapiro–Wilk tests, probability plots, and quantile plots. A two-tailed *t*-test was used to test for differences by ecosystem type for aboveground C stocks at ground-truthed sites. A Wilcoxon rank-sum test was used to test for differences by ecosystem type for modeled C stocks and for C density of surficial soil at ground-truthed sites. Two-tailed *t*-tests were used to test the difference in tree cover, NDVI, and tree height between ecosystem types across Southwest Florida. Pearson's correlation coefficient was used to assess the relationship between C stock and model predictors.

## Results

### Belowground C Model Development

The soil dataset, compiled from novel and published data, included 8459 values from 421 cores (core locations shown in Fig. 1). Soil data were evenly divided between mangroves and salt marsh/other ecosystems, with over half of the available values from the top 30 cm of soil (Fig. 2). Soil C density was generally higher in mangroves

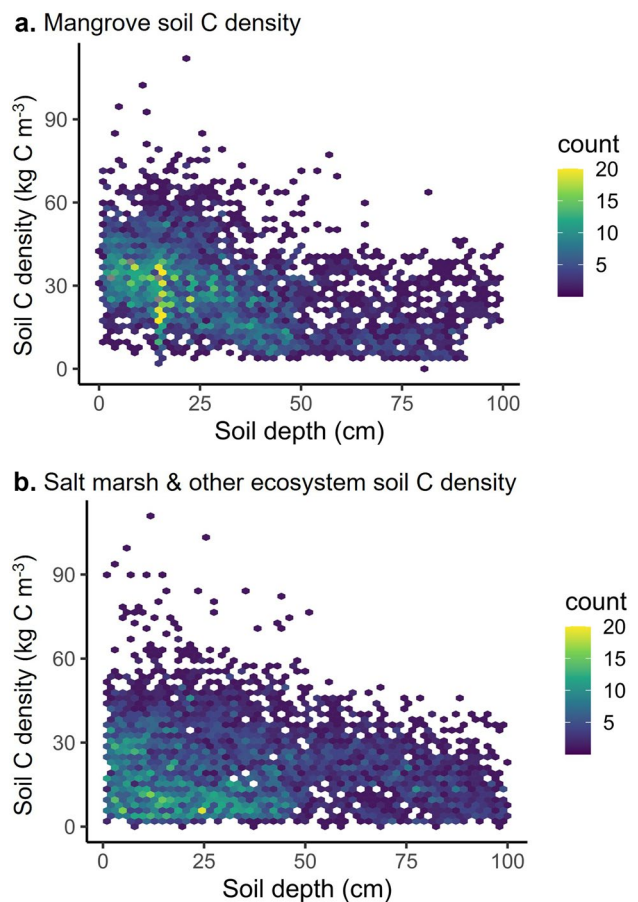
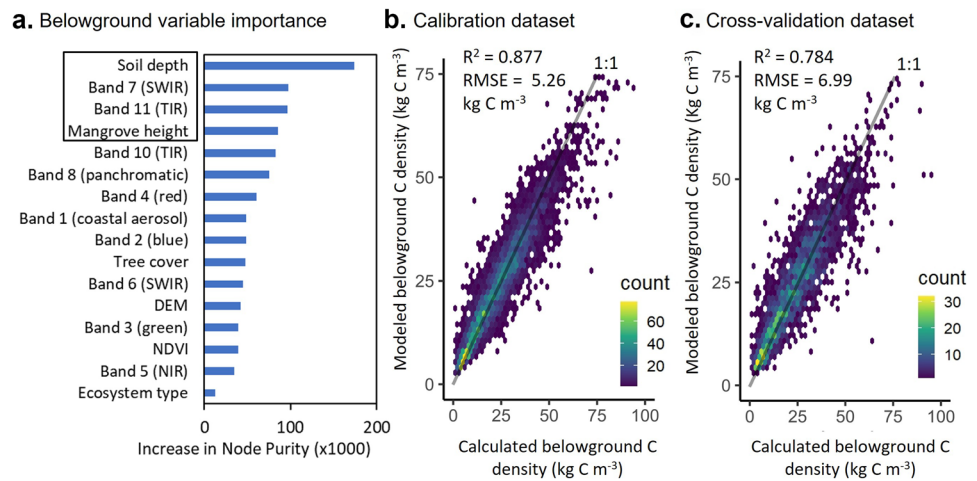


**Fig. 2** Density scatterplots depicting soil C density as a function of depth for datasets compiled from mangrove (a;  $n=4,079$  soil samples) and salt marsh and other ecosystems (b;  $n=4,383$  soil samples)

compared to salt marsh/other ecosystems, but it decreased with depth in both types of ecosystems (Fig. 2). Carbon density of surficial soils (from 0–1 cm depth) was significantly higher in mangrove ecosystems, although there was considerable overlap between the two ecosystem types (Wilcoxon rank-sum  $W=3517$ ,  $p<0.0001$ ).

The model focused on OC only and did not incorporate inorganic carbon from sources such as calcium carbonate. The four most important variables for predicting soil C density in the belowground model, in order of importance, were soil depth, Landsat 8 Band 7 (shortwave infrared; SWIR at 2.11–2.29  $\mu\text{m}$ ), Landsat 8 Band 11 (thermal infrared; TIR at 11.50–12.51  $\mu\text{m}$ ), and mangrove height (Fig. 3a); these four variables were used to generate the final random forest model predicting belowground C density. The model predicted C density with a root mean square error (RMSE) of 5.26  $\text{kg C m}^{-3}$  and  $R^2$  value of 0.877 for the calibration dataset. The cross-validation dataset had a RMSE of 6.99  $\text{kg C m}^{-3}$  and  $R^2$  value of 0.784 (Fig. 3b, c).

**Fig. 3** Variable importance (a) for predicting soil C density of calibration (b) and cross-validation (c) datasets. The top four variables in panel a were used to create the final model shown in panels b and c. Acronyms include shortwave infrared (SWIR), thermal infrared (TIR), digital elevation model (DEM), normalized difference vegetation index (NDVI), near infrared (NIR), and root-mean square error (RMSE)



## Aboveground C Model Development

The sample size for the aboveground dataset was considerably smaller and included data from 86 plots. Aboveground C stocks at the ground-truthing sites showed a clear separation based on ecosystem type (Fig. 4), with significantly higher C stocks at mangrove sites compared to salt marsh and other ecosystem types ( $t_2 = 19.145$ ,  $df = 77.385$ ,  $p < 0.0001$ ).

Four predictors were also used to create the aboveground C model: ecosystem type, percent tree cover, NDVI, and mangrove height (Fig. 5a). The random forest model predicted aboveground C stocks with an RMSE of  $9.87\ Mg\ ha^{-1}$  and  $R^2$  value of 0.864 for the calibration dataset and an RMSE of  $12.68\ Mg\ ha^{-1}$  and  $R^2$  value of 0.709 for the cross-validation dataset (Fig. 5b, c).

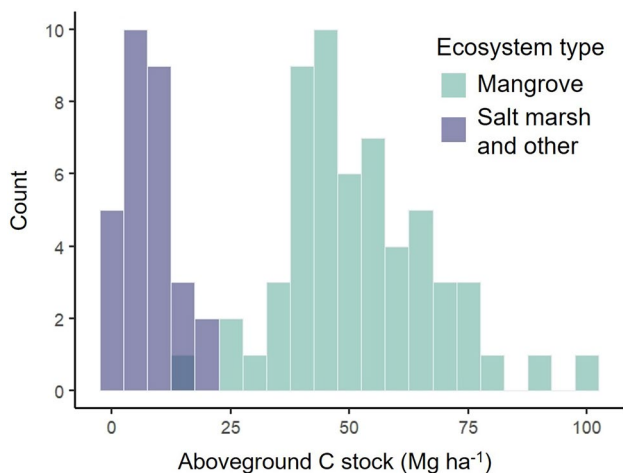


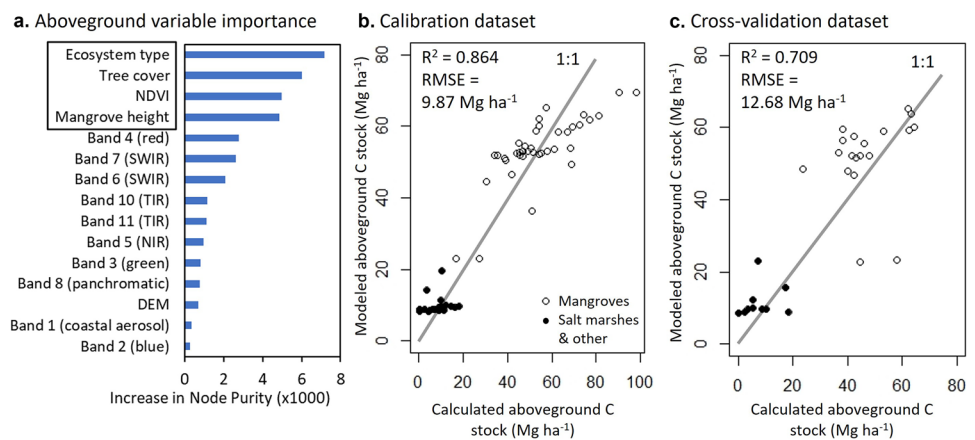
**Fig. 4** Histogram showing frequency of calculated aboveground C stocks at ground-truthing sites

## Extrapolated Models

The above- and belowground models were then used to predict C stocks at a 30-m resolution across Southwest Florida as a function of ecosystem type as determined by classification of each  $30 \times 30$ -m pixel as either mangrove swamp or salt marsh by SFWMD (2018) and SFWMD (2019) land-cover maps (Figs. 6 and 7; model results are available for online viewing and download at <https://gis.myfwc.com/SWFLCarbonStocksMap/>). Modeled aboveground C stocks in salt marshes/other ecosystems ranged from  $8.3$  to  $51.9\ Mg\ ha^{-1}$ , with a mean of  $13.4 \pm 7.5\ Mg\ ha^{-1}$  (Table 1; Figs. 5c and 7a). Pixels classified as salt marsh/other ecosystems in land-cover maps may still contain some trees (Table 1). Modeled aboveground C stocks in mangroves ranged from  $21.5$  to  $71.3\ Mg\ ha^{-1}$ , with a mean of  $46.4 \pm 14.1\ Mg\ ha^{-1}$ . The range of predicted belowground C stocks showed even more overlap than aboveground C stocks between the salt marsh/other ecosystems and mangroves (Fig. 6b). Modeled belowground C stocks in salt marshes/other ecosystems up to a depth of 1 m ranged from  $70.5$  to  $594.3\ Mg\ ha^{-1}$ , with a mean of  $273.4 \pm 70.7\ Mg\ ha^{-1}$ . Modeled belowground C stocks in mangroves ranged from  $70.7$  to  $628.9\ Mg\ ha^{-1}$ , with a mean of  $347.5 \pm 100.6\ Mg\ ha^{-1}$ . Modeled total C stocks were significantly higher in mangroves compared to salt marshes/other ecosystems (Wilcoxon rank-sum  $W = 8.1611e + 11$ ,  $p < 0.0001$ ). Both above- and belowground C stocks were also significantly greater in mangroves compared to salt marshes/other ecosystems (Fig. 8a; aboveground Wilcoxon rank sum  $W = 9.8626e + 11$ ,  $p < 0.0001$ ; belowground Wilcoxon rank sum  $W = 7.2714e + 11$ ,  $p < 0.0001$ ).

Total C stocks of both mangroves and salt marshes/other ecosystems were generally higher in the southern regions

**Fig. 5** Variable importance (a) for predicting aboveground C stocks of calibration (b) and cross-validation (c) datasets. The top four variables in panel a were used to create the final model shown in panels b and c. Both ecosystem types (mangroves, shown as open circles, and salt marshes/other ecosystems, shown as filled circles) were included in the same model



of Ten Thousand Islands and the Everglades compared to the northern regions of Tampa Bay/Sarasota Bay and Charlotte Harbor (Figs. 7 and 8b, Table 1). Total modeled C stock was negatively correlated with latitude (Pearson's  $r = -0.348$ ,  $df = 2,847,057$ ,  $p < 0.0001$ ). Aboveground C stock was positively correlated with NDVI (Pearson's  $r = 0.764$ ,  $df = 2,847,057$ ,  $p < 0.0001$ ). Mangroves were taller in the southern regions of the study area (Table 1). Tree height averaged  $11.6 \pm 7.5$  m in the Ten Thousand Islands and  $8.5 \pm 6.5$  m in the Everglades, while they were only  $6.1 \pm 4.5$  m tall in Tampa Bay and Sarasota Bay. However, percent tree cover in areas classified as mangroves was lower in southern regions (Table 1); tree cover was only  $62.4 \pm 32.3\%$  in the Everglades compared to  $75.0 \pm 29.6\%$  in Tampa Bay and Sarasota Bay (Table 1). Salt marshes/other ecosystems had lower C stocks than mangroves in each region ( $t_2$  test  $p$  values  $< 0.0001$ ). Areas classified as salt marshes/other ecosystems had significantly lower percent tree cover, maximum mangrove height, and NDVI compared to mangrove forests ( $t_2$  test  $p$  values  $< 0.0001$ ; Table 1).

In addition to latitudinal trends, C stocks and several of their predictors showed spatial trends related to distance from shore (Figs. 7 and 9). Both above- and belowground C stocks generally decreased further inland (Fig. 9a, b). Mangrove tree height and percent tree cover also declined inland (Fig. 9c, d). NDVI values were higher and SWIR values were lower closer to shore (Fig. 9e, f).

## Discussion

### Comparison with Local and Global Blue C Stocks

In this study, modeled C stock (aboveground and belowground up to 1-m depth) in Southwest Florida mangroves contained significantly higher C stocks compared to salt marshes/other ecosystems ( $393.9 \pm 107.1$  Mg C  $ha^{-1}$  and  $286.7 \pm 71.9$  Mg C  $ha^{-1}$ , respectively; Table 1).

Globally, C stocks in mangroves average  $739$  Mg C  $ha^{-1}$  and salt marshes average approximately  $334$  Mg C  $ha^{-1}$  (aboveground and belowground C up to 1-m depth; Alongi 2020). Florida mangroves do not reach the higher range of C stocks found in Indo-Pacific mangroves (Donato et al. 2011; Alongi 2014, 2020; Doughty et al. 2016; Jerath et al. 2016; Radabaugh et al. 2018). Florida has a comparatively drier and cooler climate and higher tropical cyclone frequency relative to equatorial mangroves, leading to smaller mangroves and less organic matter in the soil (Radabaugh et al. 2018; Simard et al. 2019a). Shallow peat layers ( $< 50$  cm in depth) are not uncommon in many mangrove forests in Florida, particularly in the mangrove forests found in the subtropical/temperate climate in the northern limit of Florida's mangrove range (Doughty et al. 2016; Radabaugh et al. 2018; Steinmuller et al. 2022).

Mangrove aboveground C and biomass have been modeled before, primarily with the use of tree height (Simard et al. 2006, 2019a, b; Lu et al. 2016; Fatoyinbo et al. 2018; Navarro et al. 2020). In this study, modeled aboveground C stocks in Southwest Florida mangroves ranged from  $21.5$  to  $71.3$  Mg  $ha^{-1}$ , with a mean of  $46.4 \pm 14.1$  Mg  $ha^{-1}$ . Simard et al. (2019b) modeled Florida mangrove biomass on a similar scale, with statewide values ranging from  $0.52$  to  $97.46$  Mg  $ha^{-1}$  and a mean of  $33.6 \pm 26.23$  Mg  $ha^{-1}$ . For comparison, the tallest mangrove forests in the world reach an average height of  $16.6$ – $30.7$  m (compared to  $6.1$ – $11.6$  m in Southwest FL; Table 1) and contain  $212$ – $595$  Mg  $ha^{-1}$  (Simard et al. 2019a).

Total C stocks in mangroves were highest in South Florida and increased from an average of  $265.1 \pm 43.2$  Mg  $ha^{-1}$  in Tampa Bay/Sarasota Bay to  $409 \pm 104.4$  Mg  $ha^{-1}$  in the Everglades (Table 1; Figs. 7 and 8). C stocks are lower in Tampa Bay for a variety of reasons. First, many of the mangrove forests in Tampa Bay are relatively young due to habitat switching from salt marsh to mangrove forest (Raabe et al. 2012; Jackson et al. 2021). Mangroves in Tampa Bay are also smaller trees than their counterparts in South

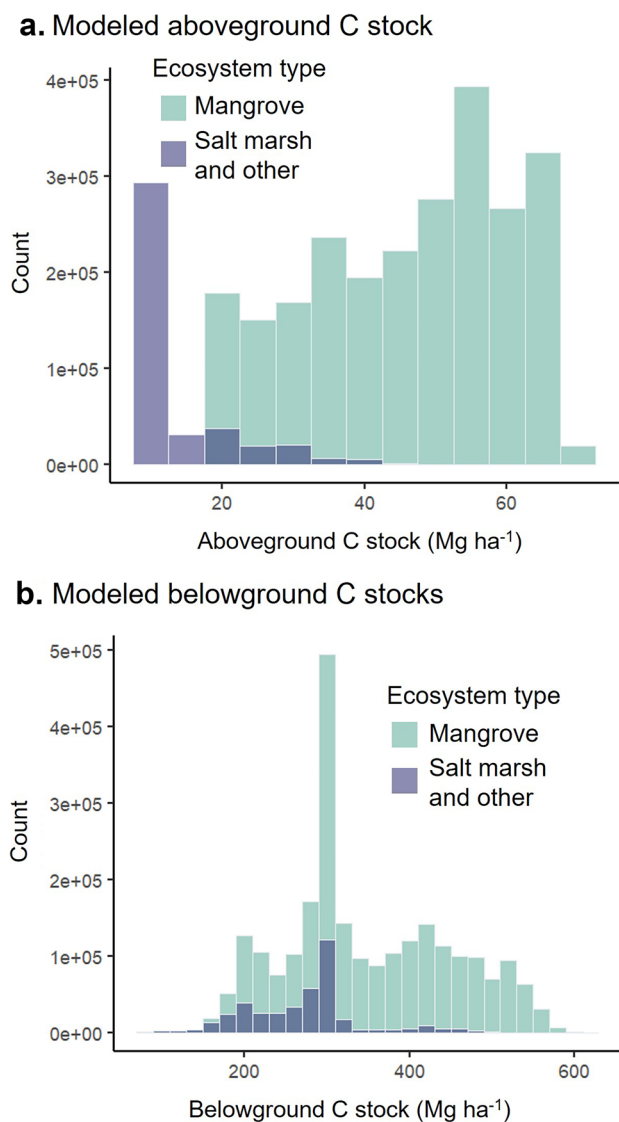


**Fig. 6** Histograms showing frequency of modeled C stocks in 30×30-m pixels across Southwest Florida for aboveground C (**a**); and belowground C up to 1-m depth (**b**)

Florida (Simard et al. 2006; Radabaugh et al. 2018). Additionally, belowground C stocks increase at lower latitudes in Florida as a result of a higher proportion of organic matter in the soil and deeper layers of peat (Cohen 1968; Doughty et al. 2016; Radabaugh et al. 2018; Toscano et al. 2018). Additionally, the mangrove soil organic matter itself has a higher proportion of OC in south Florida compared to north Florida (Breithaupt et al. 2023).

Whereas peat layers are often shallow (or absent) in Tampa Bay coastal wetlands, restricting the model to 1-m depth underestimated belowground C stocks in other areas of Southwest Florida (Kauffman et al. 2020). Peat deposits 3–4 m in depth have been found in the Shark River Slough and near Whitewater Bay in the Everglades (Cohen 1968).

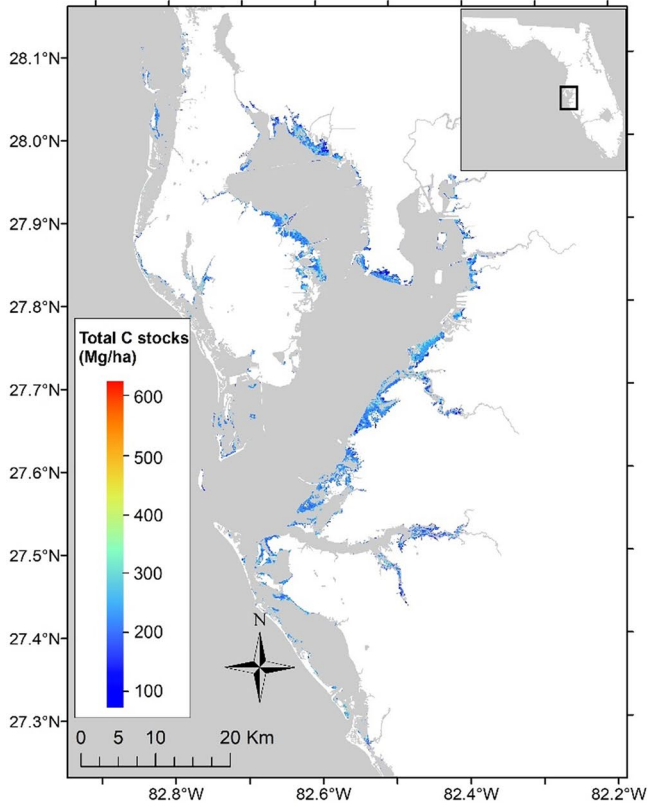
Just outside the boundaries of this study, peat deposits 5–7 m deep have been found in Swan Key south of Biscayne Bay and Snipe Key in the Lower Florida Keys (Khan et al. 2017, 2022; Toscano et al. 2018). Thus, average C stocks in Florida mangroves are likely underestimated by this model and the latitudinal trends in C stocks are likely more pronounced than this model suggests.

Carbon stocks vary widely in mangrove and salt marsh ecosystems. On a small scale (10 s to 100 s of meters), belowground C stock tends to increase with distance from shore (Fujimoto et al. 1999; Kauffman et al. 2011; Breithaupt et al. 2017; Gress et al. 2017; Ouyang et al. 2017). This trend is largely driven by increasing soil density in the landward part of the transect, resulting in greater C stocks, especially in deeper (> 50 cm) parts of the cores (Kauffman et al. 2011). On a larger scale (kilometers), this model clearly shows that C stocks decrease inland as the ecosystem changed into salt marsh or transitional ecosystems (Figs. 7 and 9). Belowground C stocks also vary among forests dominated by different mangrove species (Paolini and Sánchez-Arias 2008; Liu et al. 2014; Gress et al. 2017). Mangrove species in Florida often separate based on elevation and geomorphology (Lugo and Snedaker 1974; Rovai et al. 2018).

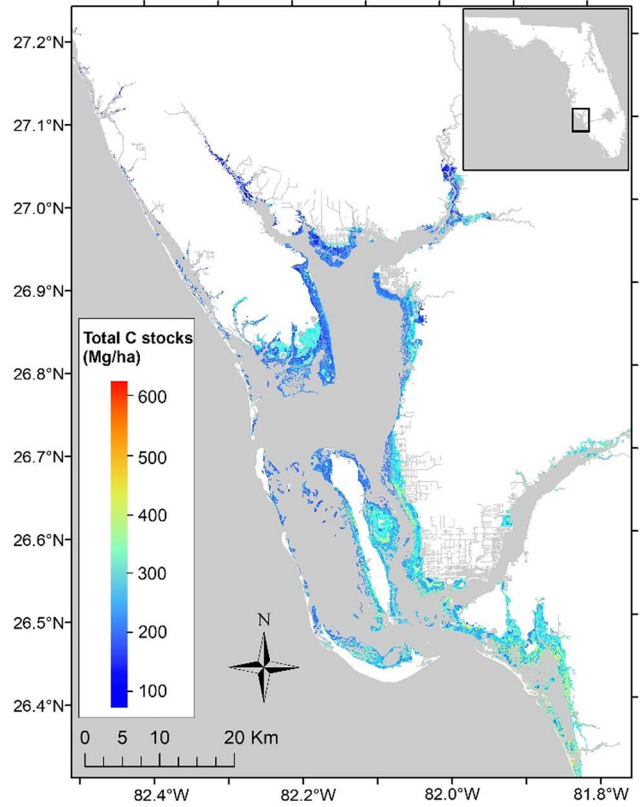
While there was a significant correlation between modeled above- and belowground C stocks of mangrove and salt marsh/other ecosystems in this study, Pearson's  $r$  value of this relationship was only 0.45. Other blue C studies in mangrove forests have found a weak or unpredictable relationship between above- and belowground C stocks (Gress et al. 2017; Kauffman et al. 2020). Belowground C stocks and C burial rates are often more dependent on rates of primary productivity, accretion, deposition of allochthonous organic matter, decomposition, and export of OC than on aboveground biomass (Bouillon et al. 2003; Maher et al. 2013; Saintilan et al. 2013; Roner et al. 2016). This emphasizes the importance of creating independent models for above- and belowground C stocks.

Carbon burial rates exhibit significant variability within and among regions of Southwest Florida. For example, the 100-year average burial rates that have been reported for the southernmost sites in the coastal Everglades mangroves range from 69 to 212  $\text{g m}^{-2} \text{yr}^{-1}$  (Breithaupt et al. 2019). Slightly north of the Everglades, rates of 20–162  $\text{g m}^{-2} \text{yr}^{-1}$  have been reported in the Ten Thousand Islands (Lynch 1989; D. Cahoon and J. Lynch, [unpublished, 1994] in Chmura et al. 2003, Schafer 2020), and rates of 47–162  $\text{g m}^{-2} \text{yr}^{-1}$  were measured in Naples Bay for sites including disturbed and natural conditions (Marchio et al. 2016). For our northernmost sites, rates of 82–185  $\text{g m}^{-2} \text{yr}^{-1}$  have been reported in Tampa Bay (Gonnea 2016). Marsh burial rates in southwest Florida are sparse in the literature, but 100-year average rates

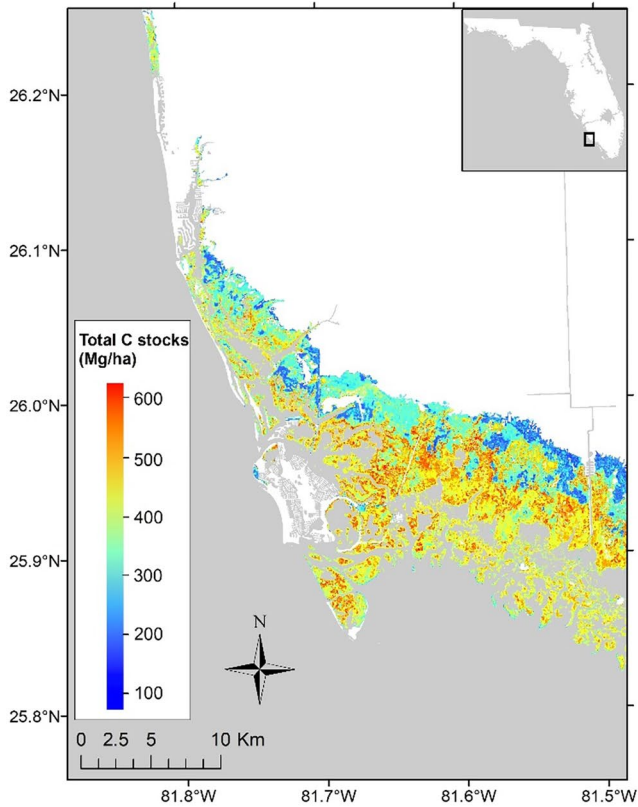
**a. Tampa Bay and Sarasota Bay**



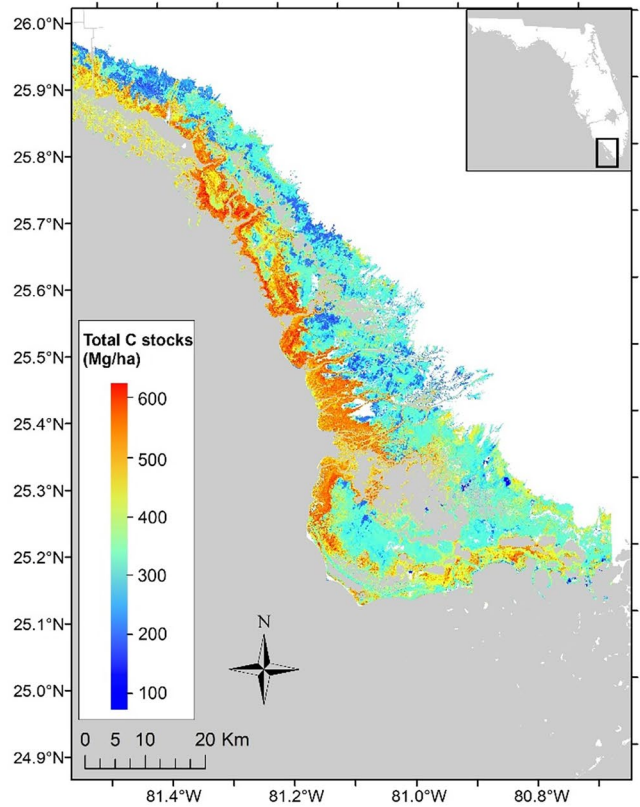
**b. Charlotte Harbor**



**c. Ten Thousand Islands**



**d. Everglades**



◀**Fig. 7** Map of total OC in coastal wetlands in Tampa Bay and Sarasota Bay (a), Charlotte Harbor (b), Ten Thousand Islands (c), and the coastal Everglades (d). Values are sums of the above- and belowground modeled C stocks at a 30-m resolution. Model results can also be viewed or downloaded online at <https://gis.myfwc.com/SWFLCarbonStocksMap/>

of 29.7 and 49.3 g m<sup>-2</sup> yr<sup>-1</sup> have been recorded for the coastal Everglades (Breithaupt et al. 2020).

### Belowground C Model

Global models of C stock in mangrove soils include Rovai et al. (2018), which found that tidal amplitude and minimum temperature explained 20% of the global variability in soil OC stocks. Sanderman et al. (2018) created a global model of mangrove soil C density based on a suite of variables with training and testing RMSEs of 6.9 and 10.9 kg C m<sup>-3</sup>, respectively. The belowground C model developed in this study offers both improved accuracy and decreased overfitting with training and testing RMSEs of 5.26 kg C m<sup>-3</sup> and 6.99 kg C m<sup>-3</sup>, respectively, while also incorporating both mangrove and salt marsh/other ecosystems. Soil depth is by far the most important factor predicting soil C density not only in coastal wetlands (Fig. 3; Sanderman et al. 2018) but also in global modeling of all terrestrial soils (Hengl et al. 2017). Unlike the aboveground model, ecosystem type was the least important predictor variable for soil C density, which is not surprising given the overlap in soil C density in mangrove and salt marsh ecosystems (Fig. 2; Steinmuller et al. 2022).

The regional focus of this study allows for optimized use of hyperspectral remote sensing data and local vegetation models to reduce RSME. In addition to depth and mangrove height, other important predictors of soil C density were SWIR (Landsat 8 Band 7) and TIR (Landsat 8 Band 11). Absorption of SWIR is an indicator of soil and vegetation wetness, while TIR is an indicator of heat. By providing information on surface temperature, TIR is useful for identifying water bodies and inundated vs. non-inundated patches of land (Leblanc et al. 2011, Amani et al. 2018, Mahdavi et al. 2018). Both SWIR and TIR have proven useful in prior studies for identifying and mapping wetland types (Amani et al. 2018, Mahdavi et al. 2018), mangrove extent and species (Shi et al. 2016; Wang et al. 2018; Baloloy et al. 2020), mangrove canopy cover (Abd-El Monsef and Smith 2017), and C stocks (Wicaksono 2017; Hickey et al. 2018). Wet and dry soil can be identified using SWIR; therefore, SWIR is useful for differentiating between wetland and non-wetland vegetation (Wang et al. 2018). In this study, absorption of SWIR was generally higher (and thus SWIR reflectance lower) in mangrove forests compared to salt marshes (Fig. 9f) due to the increased absorption of SWIR

by the high moisture content in healthy mangrove canopies (Wicaksono 2017).

### Aboveground C Model

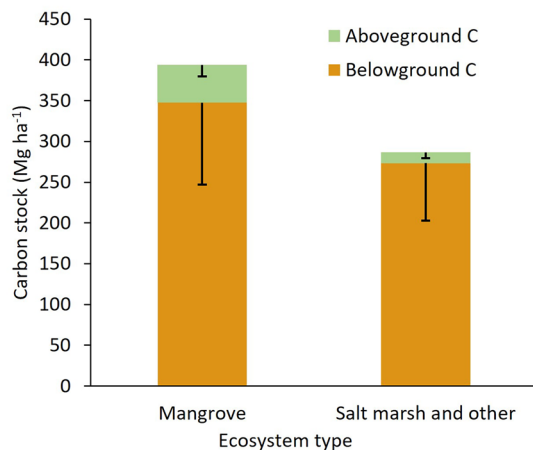
The most important factors for predicting aboveground C stocks were ecosystem type, percent tree cover, NDVI, and mangrove height. The incorporation of ecosystem type (i.e., mangrove and salt marsh/other vegetation) as a parameter allowed the model to fine-tune the remaining predictors for each ecosystem individually. Together, these four metrics provide information on the ecosystem structure (e.g., tree abundance and size) and function (e.g., type and quality). NDVI quantifies the reflection of near-infrared wavelengths by vegetation and the absorption of red wavelengths. High NDVI values indicate the presence of dense, green vegetation. Generally, low NDVI values are an indicator of moisture-stressed vegetation, values near 0.1 indicate bare soil, and negative values are indicative of water or clouds. NDVI thus provides a way to differentiate between types of vegetation, density of leaves, and other factors such as moisture stress (Carlson and Ripley 1997). As expected, NDVI had a positive correlation with modeled aboveground C stocks in this study. In other studies, NDVI proved useful to detect different species of mangroves (Valderrama-Landeros et al. 2018), density of mangrove trees (Thu and Populus 2007), dominance of live vs. dead trees (Valderrama-Landeros et al. 2018), stress and degradation in mangrove forests (Alatorre et al. 2016; Saravanan et al. 2019), and to estimate mangrove biomass (Patil et al. 2015; Winarso et al. 2017).

Salt marsh vegetation is more challenging to model than mangrove forests due to the broad variety of species, growth patterns, and density of vegetation. Several local studies have sought to model aboveground biomass or C stocks in salt marshes using lidar (e.g., Medeiros et al. 2015; Rogers et al. 2015), or lidar coupled with hyperspectral data (e.g., Kulawardhana et al. 2014; Wang et al. 2017). Large-scale modeling efforts for aboveground biomass in salt marshes rely on satellite-derived data as predictive parameters. Byrd et al. (2018) modeled aboveground C stocks in salt marshes in the conterminous United States using satellite-derived vegetation indices. The best model in Byrd et al. (2018) explained 61% of variability and was created using six vegetation indices, including NDVI, and a soil-adjusted vegetation index. The model presented here explained 86.4% and 70.9% of variability in the calibration and cross-validation datasets, respectively (Fig. 5). This improvement in  $R^2$  values is, in part, attributable to the inclusion of both salt marshes and mangroves in the model. Mangrove biomass is inherently easier to model due to quantifiable relationships with predictors such as canopy height and tree cover, and the incorporation of both mangroves and salt marshes in the

**Table 1** Means ( $\pm$  standard deviation) of selected predictors and model outputs from the above- and belowground random forest models. Belowground C is modeled to 1-m depth

Ecosystem type	Region	Model predictors				Model output					Total C stocks per region (Tg)	Pixels in model ( <i>n</i> )
		Mangrove height (m)	Tree cover (%)	NDVI	Surface (0–1 cm) soil C density ( $\text{kg C m}^{-3}$ )	Belowground C stock ( $\text{Mg C ha}^{-1}$ )	Above-ground C stock ( $\text{Mg C ha}^{-1}$ )	Total C stocks ( $\text{Mg C ha}^{-1}$ )				
Mangrove	Tampa Bay and Sarasota Bay	6.1 $\pm$ 4.5	75.0 $\pm$ 29.6	0.32 $\pm$ 0.07	33.0 $\pm$ 5.9	218.0 $\pm$ 40.2	47.1 $\pm$ 10.4	265.1 $\pm$ 43.2	2.13	89,419		
	Charlotte Harbor	6.6 $\pm$ 4.9	77.5 $\pm$ 24.9	0.31 $\pm$ 0.07	33.7 $\pm$ 5.2	251.6 $\pm$ 55.9	48.6 $\pm$ 10.6	300.2 $\pm$ 55.4	8.07	298,489		
	Ten Thousand Islands	11.6 $\pm$ 7.5	72.7 $\pm$ 28.4	0.32 $\pm$ 0.08	41.6 $\pm$ 6.4	383.6 $\pm$ 87.7	50.9 $\pm$ 14.4	434.6 $\pm$ 96.8	13.06	333,975		
Salt marsh and other	Everglades	8.9 $\pm$ 6.5	62.4 $\pm$ 32.3	0.31 $\pm$ 0.09	40.1 $\pm$ 6.4	364.0 $\pm$ 96.1	45.0 $\pm$ 14.5	409.0 $\pm$ 104.4	62.93	1,709,718		
	All	8.9 $\pm$ 6.5	66.1 $\pm$ 31.4	0.31 $\pm$ 0.08	39.2 $\pm$ 6.7	347.5 $\pm$ 100.6	46.4 $\pm$ 14.1	393.9 $\pm$ 107.1	86.19	2,431,601		
	Tampa Bay and Sarasota Bay	0.6 $\pm$ 2.1	50.0 $\pm$ 28.6	0.25 $\pm$ 0.08	25.9 $\pm$ 7.4	184.2 $\pm$ 51.4	15.8 $\pm$ 8.0	199.9 $\pm$ 53.1	0.45	25,074		
Mangrove	Charlotte Harbor	0.6 $\pm$ 2.1	39.3 $\pm$ 30.1	0.23 $\pm$ 0.08	32.6 $\pm$ 5.4	253.4 $\pm$ 58.0	14.4 $\pm$ 7.7	267.8 $\pm$ 57.5	1.43	59,134		
	Ten Thousand Islands	0.9 $\pm$ 2.7	20.7 $\pm$ 29.0	0.19 $\pm$ 0.08	31.1 $\pm$ 5.8	267.2 $\pm$ 76.2	12.3 $\pm$ 7.4	279.5 $\pm$ 78.7	2.79	110,805		
	Everglades	1.4 $\pm$ 3.1	22.0 $\pm$ 26.7	0.22 $\pm$ 0.07	34.6 $\pm$ 4.5	291.9 $\pm$ 62.7	13.3 $\pm$ 7.4	305.3 $\pm$ 64.1	6.06	220,445		
All	1.1 $\pm$ 2.9	25.8 $\pm$ 29.2	0.21 $\pm$ 0.08	32.9 $\pm$ 5.7	273.4 $\pm$ 70.7	13.4 $\pm$ 7.5	286.7 $\pm$ 71.9	10.72	415,458			

**a. Modeled carbon stock across ecosystem types in Southwest Florida**



**b. Carbon stock across ecosystem types and regions in Southwest Florida**

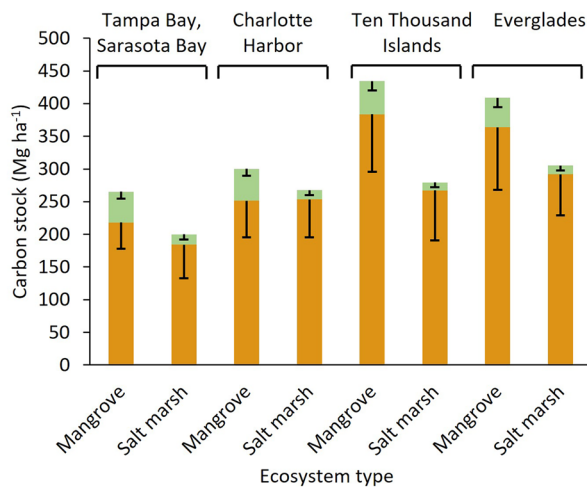


**Fig. 8** Modeled above- and belowground C stocks across ecosystem types (a) and ecosystem types and regions (b) in Southwest Florida. Error bars show standard deviation and are shown in negative direction only for clarity

model enables ecosystem type to predict a large degree of variance. The model does not require any estimate of salt marsh vegetation height, which has been a notably difficult variable to quantify given the short and dense nature of the vegetation in salt marshes (Hladik and Alber 2012; Medeiros et al. 2015).

The location and ecosystem type of the ground truthing sites were not necessarily proportionate to the areal coverage of the variety of salt marshes and mangroves found across all of Southwest Florida. However, averaged ground truthing and model datasets resulted in similar values. For instance, average aboveground mangrove C stock for the ground truthing dataset was  $51.93 \pm 15.6 \text{ Mg ha}^{-1}$  for mangroves, while the average for mangroves in the model was

$46.4 \pm 14.1 \text{ Mg ha}^{-1}$ . Average aboveground C stock for salt marshes/other ecosystems was  $7.81 \pm 5.5 \text{ Mg ha}^{-1}$  while the average in the model was  $13.4 \pm 7.5 \text{ Mg ha}^{-1}$ .

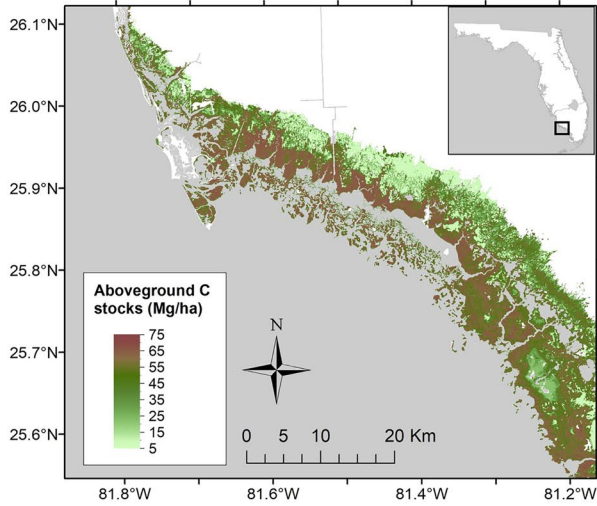
### Sources of Error

Discrepancies between the spatial and temporal resolution of ground-truthing data and remote-sensing predictors introduced some inherent error in the models. Whereas all remote-sensing predictors considered for the model were available at a 30-m resolution, the soil cores used to model soil C density were point data. Using point data to represent a  $30 \times 30\text{-m}$  area does require some assumption of stratigraphic homogeneity. Likewise, the vegetation data used to estimate aboveground C stocks were collected from multiple circular plots along a 100-m transect (following Howard et al. 2014) or from  $10 \times 10\text{-m}$  plots. Thus, the spatial resolution of the field data was either larger or smaller (depending on the sampling method) than the resolution of the satellite imagery. While a direct pairing of spatial scale between the two datasets would likely improve modeling efforts, other studies have found that it is still possible to join multiple datasets for C stock modeling purposes despite differences in spatial resolution (Hengl et al. 2017; Wicaksono 2017; Sanderman et al. 2018; Simard et al. 2019a).

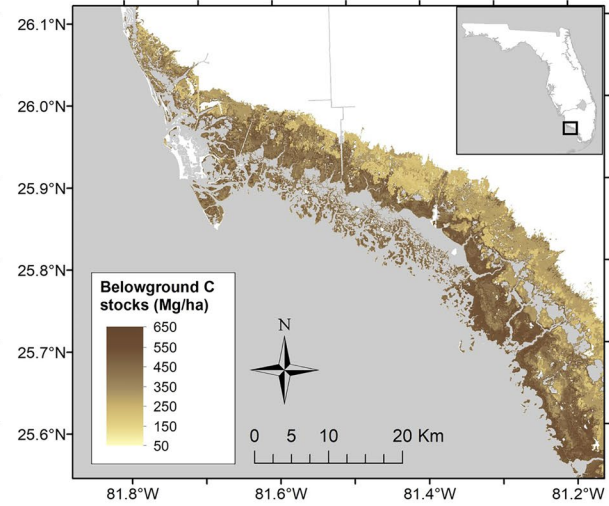
Land-cover mapping also introduces a degree of error, as it classifies complex vegetation distributions into simplified categories. The minimum mapping unit for wetlands in Water Management District Land Use Land Cover maps is 0.2 ha (SFWMD 2018, SFWMD 2019). In this mapping, coastal wetland parcels that contain both salt marsh and mangrove vegetation were classified as the vegetation type that occupied the greatest proportion of the area. This can lead to underrepresentation of mangroves in land cover classification schemes, as mangroves often grow as patches or fringes in salt marshes, particularly at the edges of their distribution (Bardou et al. 2023). The patchiness of mangrove growth (and presence of woody vegetation, such as *B. halimifolia* in salt marshes) could explain why areas classified as salt marshes in Southwest Florida contained 22–50% tree cover, and why areas classified as mangrove forests contained less than 100% tree cover (Table 1).

Not all vegetation present in coastal wetlands will be visible from an aerial view, and thus it cannot all be detected using remote-sensing platforms. Whereas the shrubs, seedlings, and fallen dead wood are often included in blue C accounting protocols for mangrove forests, it is generally not possible to detect these understory components via remote sensing. The thickness of the canopy makes it difficult to include sub-canopy vegetation in biomass estimates derived from canopy height or remote sensing data (Wicaksono 2017). However, most mature mangrove forests have minimal understory compared to terrestrial forests (Smith 1993),

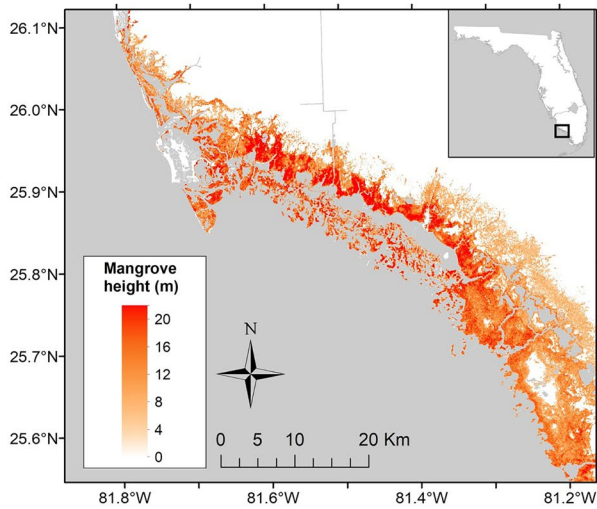
**a.** Aboveground carbon stocks



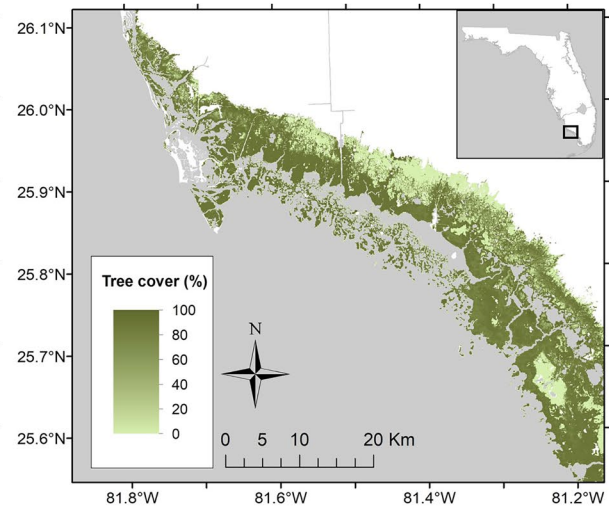
**b.** Belowground carbon stocks



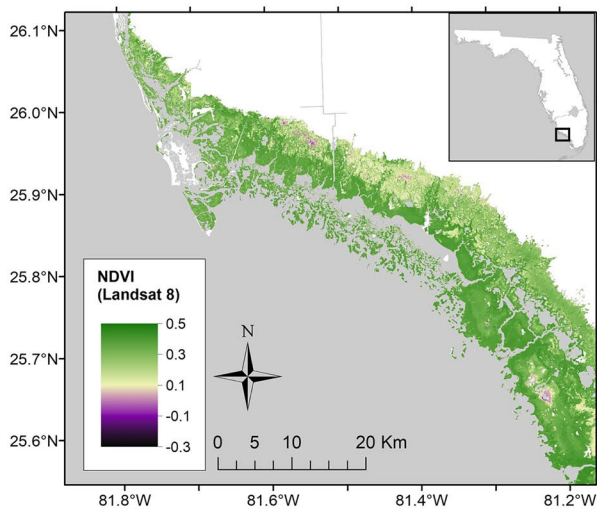
**c.** Maximum mangrove height



**d.** Percent tree cover



**e.** NDVI



**f.** Shortwave infrared

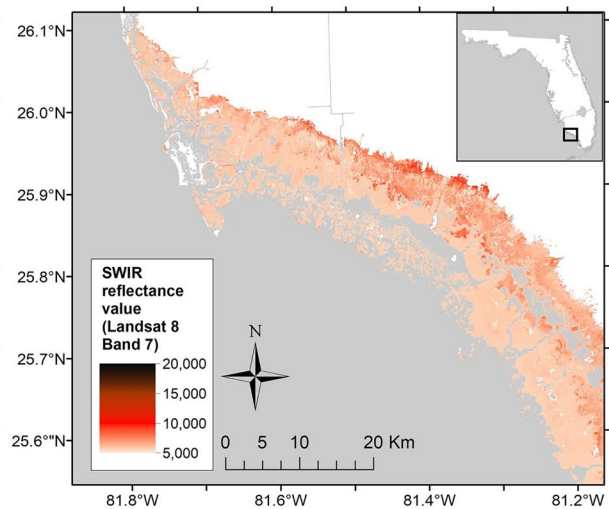


**Fig. 9** Maps of modeled aboveground C (a) and belowground C to 1-m depth (b) in the Ten Thousand Islands region of Southwest Florida. Predictors for the models included maximum mangrove height from Simard et al. (2019b) (c), percent tree canopy cover from Hansen et al. (2013) (d), NDVI (e, from Landsat 8), and shortwave infrared reflectance (f, from Landsat 8 Band 7)

so the biomass contribution of the understory is small relative to that of mature trees. Understory seedlings and shrubs comprised only  $1.2 \pm 2.0\%$  of the total aboveground C stocks in the 14 mangrove sites sampled for this study, and only  $1.5 \pm 0.3\%$  of aboveground C stocks in Tampa Bay mangroves (Radabaugh et al. 2018).

Temporal variability in collection of ground-truthing data and remote-sensing data may also impact the fit of the model. The images used for the Water Management District maps used in this model were collected in 2014–2017. The tree cover data were obtained from Hansen et al. (2013), which modeled tree cover in the year 2000. The mangrove height data from Simard et al. (2019b) were calculated for the nominal year 2000, while the Landsat 8 data used for the modeling were collected in 2015. The aboveground ground-truthing dataset was based on field work conducted between 2015 and 2020, and cores were collected for the belowground dataset from 1995 to 2020. Locations that had markedly different aboveground C stocks than expected (Fig. 5) may have had either increased or decreased abundance of woody vegetation between the time of ground truthing and the time of remote-sensing data collection.

Habitat switching between salt marshes and mangroves is in continuous flux in Florida as a result of temperature fluctuations and sea-level rise, with mangroves generally encroaching into salt marshes in the time frame of interest in this study (2000–2020) (Krauss et al. 2011; Cavanaugh et al. 2014). Mangrove extent in the Ten Thousand Islands, for instance, increased by 35% from 1925 to 2005 (Krauss et al. 2011). Cold events impact both the spatial extent and spectral characteristics of mangrove forests (Cavanaugh et al. 2014; Zhang et al. 2016; Bardou et al. 2023). Winter cold events, such as the ones that occurred in Florida in 2010 (Zhang et al. 2016), may introduce some variability in spectral signatures in the compilation of data used to create the model.

Mangrove extent is also temporally variable due to hurricanes. The ground-truthing and remote sensing data used in this study were compiled to avoid the influence of Hurricane Irma (2017), given the temporal and spatial variability in mangrove coverage that occurred in Southwest Florida thereafter (McCarthy et al. 2020; Osland et al. 2020; Radabaugh et al. 2020; Lagomasino et al. 2021). Other storms such as Hurricanes Charlie and Wilma (which made landfall in Southwest Florida in 2004 and 2005, respectively) impacted the extent of mangrove coverage in the region (Zhang et al.

2016; Han et al. 2018; Peneva-Reed et al. 2021). However, the tree cover and mangrove height data used in this study were collected well before (around the year 2000) and remote sensing and mapping data were collected well after these hurricanes (2015–2017). Following the 2004–2005 hurricanes, most of the mangrove forest in South Florida recovered by 2008 (Han et al. 2018). Because the mangrove forests had a decade to recover, Hurricanes Charlie and Wilma are not expected to have a large influence on the data sets used for this model, with the possible exception of mangroves that failed to recover as a result of additional stress such as altered hydrology (Peneva-Reed et al. 2021).

### Long-term Stability of C Stocks

Total C stocks were generally greatest in the lower latitudes of Florida, particularly in mangroves near the coast (Fig. 7). The proximity of these mangroves to the coast also makes them vulnerable to the impacts of sea-level rise and hurricane damage. The future of C stocks in Southwest Florida (and globally) depends on ecosystem stability in the face of stressors brought about by climate change, sea-level rise, altered hydrology, and hurricanes (Smith et al. 2009; Smoak et al. 2013; Macreadie et al. 2019; Osland et al. 2020). In addition to vegetative stress as a result of increased inundation, saltwater intrusion associated with sea-level rise also changes the physicochemical conditions of soil, which can stress the limits of salt tolerance of vegetation and accelerate the rate of organic matter transformation and decomposition (Chambers et al. 2011, 2013, 2014; White and Kaplan 2017; Wilson et al. 2018). The retention of C stocks within these ecosystems will also depend largely on the ability of wetlands to accrete sediment at a rate meeting or exceeding the rate of sea-level rise (McKee 2011; Smoak et al. 2013).

Estimates of accretion rates in Florida mangroves vary widely and are highly dependent on location (Jones et al. 2019). Some evidence of increasing rates of accretion and C burial in the face of sea-level rise has been found in Southwest Florida (Jones et al. 2019; Breithaupt et al. 2020). However, it is expected that mangroves will not be able to sustain accretion rates necessary to keep up with accelerating sea-level rise once rates exceed  $6.1 \text{ mm yr}^{-1}$  (Saintilan et al. 2020). If a wetland fails to accrete soil at a sufficient rate or if the vegetation succumbs to chronic or acute stressors, the ecosystems and their associated C stocks are at risk of instability or collapse (Ellison and Stoddart 1991). Root growth is a key component of peat accumulation and stability, so vegetation mortality and the resulting loss of live root biomass can cause a loss of soil substrate and elevation (Cahoon et al. 2003; Whelan 2005; Krauss et al. 2018; Chambers et al. 2019; Radabaugh et al. 2021). This loss of elevation can, in turn, cause increased hydrologic stress for the vegetation, resulting in further mortality and elevation

loss (Lewis III et al. 2016; Krauss et al. 2018; Andres et al. 2019; Cahoon et al. 2019). Coastal wetlands that succumb to this trend of vegetation mortality and peat collapse following disturbances such as hurricanes or altered hydrology can turn into mud flats (Smith et al. 2009; Lewis III et al. 2016; Osland et al. 2020), resulting in remineralization of belowground C stocks.

Rates of sequestration and C stocks may also increase in parts of Southwest Florida as a result of mangrove expansion into salt marsh habitat. Mangroves have significantly greater above- and belowground C stocks compared to salt marshes (Fig. 8), so the increase of C sequestration that occurs as mangrove coverage increases may help counterbalance loss of C and coastal wetlands due to the stressors mentioned above. However, the impacts on belowground C will vary by region. Belowground C stock depends as much upon plant productivity, geomorphic characteristics, soil chemistry, and rates of decomposition as on aboveground biomass (Charles et al. 2020; Osland et al. 2022). Whereas some studies do indicate that mangrove encroachment will increase belowground C stocks (Doughty et al. 2016; Simpson et al. 2019), other studies do not show evidence of a significant impact (Henry and Twilley 2013; Macy et al. 2021; Steinmuller et al. 2022). Continued study of accretion, ecosystem stability, habitat switching, and C cycling will be necessary to understand the ultimate effects of climate change and its associated impacts on C stocks in Southwest Florida coastal wetlands.

## Conclusion

The regional nature of this study enabled model development with improved accuracy to predict blue C stocks in the complex coastal wetlands of Southwest Florida. The frequent intermixing of mangroves with salt marsh vegetation, variety in mangrove height, and the diverse array of herbaceous vegetation and occasional woody plants found in Florida's salt marshes and transitional ecosystems necessitates consideration of a wide variety of plant species and characteristics to accurately calculate and model aboveground C stocks. The local model also improves upon global soil C models to predict the widely variable belowground C stocks.

Southwest Florida contains over half of Florida's remaining coastal wetlands and stores approximately 96 Tg of C (Table 1). The stability of Southwest Florida's coastal wetlands and their C stocks will depend on the ability of these ecosystems and their peat deposits to withstand chronic stress resulting from sea-level rise, climate change, and altered hydrology as well as the acute stress caused by hurricanes and other disturbances.

**Supplementary Information** The online version contains supplementary material available at <https://doi.org/10.1007/s12237-023-01217-7>.

**Funding** This work was supported by Interagency Climate Change NASA program grant no. 2017–67003-26482/project accession no. 1012260 from the USDA National Institute of Food and Agriculture. Field and laboratory assistance was provided by CS Adams, M Bownick, S Harttung, S Hearne, M Osgood, E Ritz, S Roussopoulos, C Schafer, and E Wennick. Site access to the Rookery Bay National Estuarine Research Reserve was facilitated by B Jessen. Site access to the Fakahatchee Strand State Preserve was granted by the Florida Dept. of Environmental Protection (permit 02051814). The ArcGIS Experience Builder online model was created by F Alexander.

**Data Availability** Model results can also be viewed or downloaded online at <https://gis.myfwc.com/SWFLCarbonStocksMap/>. In accordance with the State of Florida's broad public records dissemination laws, all FWC data are publicly available upon request.

## References

- Abd-El Monsef, H., and S.E. Smith. 2017. A new approach for estimating mangrove canopy cover using Landsat 8 imagery. *Computers and Electronics in Agriculture* 135: 183–194. <https://doi.org/10.1016/j.compag.2017.02.007>.
- Alatorre, L.C., S. Sánchez-Carrillo, S. Miramontes-Beltrán, R.J. Medina, M.E. Torres-Olave, L.C. Bravo, L.C. Wiebe, A. Granados, D.K. Adams, E. Sánchez, and M. Uc. 2016. Temporal changes of NDVI for qualitative environmental assessment of mangroves: Shrimp farming impact on the health decline of the arid mangroves in the Gulf of California (1990–2010). *Journal of Arid Environments* 125: 98–109. <https://doi.org/10.1016/j.jaridenv.2015.10.010>.
- Alongi, D.M. 2012. Carbon sequestration in mangrove forests. *Carbon Management* 3 (3): 313–322. <https://doi.org/10.4155/cmt.12.20>.
- Alongi, D.M. 2013. Mangrove-microbe-soil relations, in interactions between macro- and microorganisms in marine sediments, edited by E. Kristensen, R.R. Haese, and J.E. Kostka, pp. 85–103, AGU, Washington, D.C. <https://doi.org/10.1029/CE060p0085>.
- Alongi, D.M. 2014. Carbon cycling and storage in mangrove forests. *Annual Review of Marine Science* 6: 195–219. <https://doi.org/10.1146/annurev-marine-010213-135020>.
- Alongi, D.M. 2020. Carbon balance in salt marsh and mangrove ecosystems: A global synthesis. *Journal of Marine Science and Engineering* 8 (10): 767. <https://doi.org/10.3390/jmse8100767>.
- Amani, M., B. Salehi, S. Mahdavi, and B. Brisco. 2018. Spectral analysis of wetlands using multi-source optical satellite imagery. *ISPRS Journal of Photogrammetry and Remote Sensing* 144: 119–136. <https://doi.org/10.1016/j.isprsjprs.2018.07.005>.
- Andres, K., M. Savarese, B. Bovard, and M. Parsons. 2019. Coastal wetland geomorphic and vegetative change: Effects of Sea-level rise and water management on brackish marshes. *Estuaries and Coasts* 42: 1308–1327. <https://doi.org/10.1007/s12237-019-00538-w>.
- Ball, D.F. 1964. Loss-on-ignition as estimate of organic matter and organic carbon in non-calcareous soils. *Journal of Soil Science* 15 (1): 84–92. <https://doi.org/10.1111/j.1365-2389.1964.tb00247.x>.
- Baloloy, A.B., A.C. Blanco, R.R.C.S. Ana, and K. Nadaoka. 2020. Development and application of a new mangrove vegetation index (MVI) for rapid and accurate mangrove mapping. *ISPRS Journal of Photogrammetry and Remote Sensing* 166: 95–117. <https://doi.org/10.1016/j.isprsjprs.2020.06.001>.

- Bardou, R., M.J. Osland, S. Scyphers, C. Shepard, et al. 2023. Rapidly changing range limits in a warming world: critical data limitations and knowledge gaps for advancing understanding of mangrove range dynamics. *Estuaries and Coasts* <https://doi.org/10.1007/s12237-023-01209-7>.
- Bauer, J.E., W.J. Cai, P.A. Raymond, T.S. Bianchi, C.S. Hopkinson, and P.A.G. Regnier. 2013. The changing carbon cycle of the coastal ocean. *Nature* 504 (7478): 61–70. <https://doi.org/10.1038/nature12857>.
- Bengtsson, L., and M. Enell. 1986. Chemical analysis. In *Handbook of Holocene Palaeoecology and Palaeohydrology*, ed. B.E. Berglund, 423–451. New Jersey: Caldwell Press.
- Bouillon, S., A.V. Borges, E. Castañeda-Moya, K. Diele, T. Dittmar, N.C. Duke, E. Kristensen, S.Y. Lee, C. Marchand, J.J. Middelburg, and V.H. Rivera-Monroy. 2008. Mangrove production and carbon sinks: a revision of global budget estimates. *Global Biogeochemical Cycles* 22 (2). <https://doi.org/10.1029/2007GB003052>.
- Bouillon, S., F. Dahdouh-Guebas, A.V.V.S. Rao, N. Koedam, and F. Dehairs. 2003. Sources of organic carbon in mangrove sediments: Variability and possible ecological implications. *Hydrobiologia* 495: 33–39. <https://doi.org/10.1023/A:1025411506526>.
- Breithaupt, J.L., J.M. Smoak, T.S. Bianchi, D.R. Vaughn, C.J. Sanders, K.R. Radabaugh, M.J. Osland, L.C. Feher, J.C. Lynch, D.R. Cahoon, and G.H. Anderson. 2020. Increasing rates of carbon burial in southwest Florida coastal wetlands. *Journal of Geophysical Research: Biogeosciences* 125 (2): e2019JG005349. <https://doi.org/10.1029/2019JG005349>.
- Breithaupt, J.L., J.M. Smoak, V.H. Rivera-Monroy, E. Castañeda-Moya, R.P. Moyer, M. Simard, and C.J. Sanders. 2017. Partitioning the relative contributions of organic matter and mineral sediment to accretion rates in carbonate platform mangrove soils. *Marine Geology* 390: 170–180. <https://doi.org/10.1016/j.margeo.2017.07.002>.
- Breithaupt, J.L., J.M. Smoak, C.J. Sanders, and T.G. Troxler. 2019. Spatial variability of organic carbon, CaCO<sub>3</sub> and nutrient burial rates spanning a mangrove productivity gradient in the coastal Everglades. *Ecosystems* 22: 844–858.
- Breithaupt, J.L., J.M. Smoak, T.J. Smith, and C.J. Sanders. 2014. Temporal variability of carbon and nutrient burial, sediment accretion, and mass accumulation over the past century in a carbonate platform mangrove forest of the Florida Everglades. *Journal of Geophysical Research: Biogeosciences* 119 (10): 2032–2048. <https://doi.org/10.1002/2014JG002715>.
- Breithaupt, J.L., H.E. Steinmuller, A.S. Rovai, K.M. Engelbert, J.M. Smoak, L.G. Chambers, S.A. Harttung, K.R. Radabaugh, R.P. Moyer, A. Chappel, D.R. Vaughn, T.S. Bianchi, R.R. Twilley P. Pagliosa, M. Cifuentes-Jara, and D. Torres. 2023. An improved framework for estimating organic carbon content of mangrove soils using loss-on-ignition and coastal environmental setting. *Wetlands* <https://doi.org/10.1007/s13157-023-01698-z>.
- Byrd, K.B., L. Ballanti, N. Thomas, D. Nguyen, J.R. Holmquist, M. Simard, and L. Windham-Myers. 2018. A remote sensing-based model of tidal marsh aboveground carbon stocks for the conterminous United States. *ISPRS Journal of Photogrammetry and Remote Sensing* 139: 255–271. <https://doi.org/10.1016/j.isprsjprs.2018.03.019>.
- Cahoon, D.R., and J.C. Lynch. 1997. Vertical accretion and shallow subsidence in a mangrove forest of southwestern Florida, USA. *Mangroves and Salt Marshes* 1 (3): 173–186. <https://doi.org/10.1023/A:1009904816246>.
- Cahoon, D.R., J.C. Lynch, C.T. Roman, J.P. Schmit, and D.E. Skidds. 2019. Evaluating the relationship among wetland vertical development, elevation capital, sea-level rise, and tidal marsh sustainability. *Estuaries and Coasts* 42: 1–15. <https://doi.org/10.1007/s12237-018-0448-x>.
- Cahoon, D.R., P. Hensel, J. Rybczyk, K.L. McKee, C.E. Proffitt, and B.C. Perez. 2003. Mass tree mortality leads to mangrove peat collapse at Bay Islands, Honduras after Hurricane Mitch. *Journal of Ecology* 91 (6): 1093–1105. <https://doi.org/10.1046/j.1365-2745.2003.00841.x>.
- Campbell, A.D., T. Fatoyinbo, S.P. Charles, L.L. Bourgeau-Chavez, J. Goes, H. Gomes, M. Halabisky, J. Holmquist, S. Lohrenz, C. Mitchell, and L.M. Moskal. 2022. A review of carbon monitoring in wet carbon systems using remote sensing. *Environmental Research Letters* 17: 025009.
- Carlson, T.N., and D.A. Ripley. 1997. On the relation between NDVI, fractional vegetation cover, and leaf area index. *Remote Sensing of Environment* 62 (3): 241–252. [https://doi.org/10.1016/S0034-4257\(97\)00104-1](https://doi.org/10.1016/S0034-4257(97)00104-1).
- Cavanaugh, K.C., J.R. Kellner, A.J. Forde, D.S. Gruner, J.D. Parker, W. Rodriguez, and I.C. Feller. 2014. Poleward expansion of mangroves is a threshold response to decreased frequency of extreme cold events. *Proceedings of the National Academy of Sciences* 111 (2): 723–727. <https://doi.org/10.1073/pnas.1315800111>.
- Chambers, L.G., S.E. Davis, T. Troxler, J.N. Boyer, A. Downey-Wall, and L.J. Scinto. 2014. Biogeochemical effects of simulated sea level rise on carbon loss in an Everglades mangrove peat soil. *Hydrobiologia* 726 (1): 195–211. <https://doi.org/10.1007/s10750-013-1764-6>.
- Chambers, L.G., T.Z. Osborne, and K.R. Reddy. 2013. Effect of salinity-altering pulsing events on soil organic carbon loss along an intertidal wetland gradient: A laboratory experiment. *Biogeochemistry* 115 (1): 363–383. <https://doi.org/10.1007/s10533-013-9841-5>.
- Chambers, L.G., K.R. Reddy, and T.Z. Osborne. 2011. Short-term response of carbon cycling to salinity pulses in a freshwater wetland. *Soil Science Society of America Journal* 75 (5): 2000–2007. <https://doi.org/10.2136/sssaj2011.0026>.
- Chambers, L.G., H.E. Steinmuller, and J.L. Breithaupt. 2019. Toward a mechanistic understanding of “peat collapse” and its potential contribution to coastal wetland loss. *Ecology* e02720. <https://doi.org/10.1002/ecy.2720>.
- Charles, S.P., J.S. Kominoski, A.R. Armitage, H. Guo, C.A. Weaver, and S.C. Pennings. 2020. Quantifying how changing mangrove cover affects ecosystem carbon storage in coastal wetlands. *Ecology* 100 (2): e02916. <https://doi.org/10.1002/ecy.2916>.
- Chen, R., and R.R. Twilley. 1999. A simulation model of organic matter and nutrient accumulation in mangrove wetland soils. *Biogeochemistry* 44 (1): 93–118. <https://doi.org/10.1007/BF00993000>.
- Chmura, G.L., S.C. Anisfeld, D.R. Cahoon, and J.C. Lynch. 2003. Global carbon sequestration in tidal, saline wetland soils. *Global Biogeochemical Cycles* 17 (4): 22–1–12. <https://doi.org/10.1029/2002GB001917>.
- Cohen, A.D. 1968. The petrology of some peats of Southern Florida (with special reference to the origin of Coals). Ph.D. Dissertation, The Pennsylvania State University, University Park, Pennsylvania.
- Craft, C.B., E.D. Seneca, and S.W. Broome. 1991. Loss on ignition and Kjeldahl digestion for estimating organic carbon and total nitrogen in estuarine marsh soils: Calibration with dry combustion. *Estuaries* 14 (2): 175–179. <https://doi.org/10.2307/1351691>.
- Dean, W.E. 1974. Determination of carbonate and organic matter in calcareous sediments and sedimentary rocks by loss on ignition; comparison with other methods. *Journal of Sedimentary Research* 44 (1): 242–248. <https://doi.org/10.1306/74D729D2-2B21-11D7-8648000102C1865D>.
- Donato, D.C., J.B. Kauffman, D. Murdiyarso, S. Kurnianto, M. Stidham, and M. Kanninen. 2011. Mangroves among the most carbon-rich forests in the tropics. *Nature Geoscience* 4 (5): 293–297. <https://doi.org/10.1038/ngeo1123>.

- Doughty, C.L., J.A. Langley, W.S. Walker, I.C. Feller, R. Schaub, and S.K. Chapman. 2016. Mangrove range expansion rapidly increases coastal wetland carbon storage. *Estuaries and Coasts* 39 (2): 385–396. <https://doi.org/10.1007/s12237-015-9993-8>.
- Ellison, J.C., and D.R. Stoddart. 1991. Mangrove ecosystem collapse during predicted sea-level rise: Holocene analogues and implications. *Journal of Coastal Research* 7 (1): 151–165.
- Enwright, N.M., L. Wang, S.M. Borchert, R.H. Day, L.C. Feher, and M.J. Osland. 2017. The impact of lidar elevation uncertainty on mapping intertidal habitats on barrier islands. *Remote Sensing* 10 (1): 5.
- Ewe, S.M., E.E. Gaiser, D.L. Childers, D. Iwaniec, V.H. Rivera-Monroy, and R.R. Twilley. 2006. Spatial and temporal patterns of aboveground net primary productivity (ANPP) along two freshwater-estuarine transects in the Florida Coastal Everglades. *Hydrobiologia* 569 (1): 459–474.
- Ewers Lewis, C.J., P.E. Carnell, J. Sanderman, J.A. Baldock, and P.I. Macreadie. 2018. Variability and vulnerability of coastal 'blue carbon' stocks: A case study from southeast Australia. *Ecosystems* 21 (2): 263–279. <https://doi.org/10.1007/s10021-017-0150-z>.
- Fatoyinbo, T., E.A. Feliciano, D. Lagomasino, S.K. Lee, and C. Trettin. 2018. Estimating mangrove aboveground biomass from airborne Lidar data: a case study from the Zambezi River delta. *Environmental Research Letters* 13 (2): 025012. <https://doi.org/10.1088/1748-9326/aa9f03>.
- Feagin, R.A., I. Forbrich, T.P. Huff, J.G. Barr, J. Ruiz-Plancarte, J.D. Fuentes, R.G. Najjar, R. Vargas, A. Vázquez-Lule, L. Windham-Myers, and K.D. Kroeger. 2020. Tidal wetland gross primary production across the continental United States, 2000–2019. *Global Biogeochemical Cycles* 34 (2): e2019GB006349. <https://doi.org/10.1029/2019GB006349>.
- Fujimoto, K., A. Imaya, R. Tabuchi, S. Kuramoto, H. Utsugi, and T. Murofushi. 1999. Belowground carbon storage of Micronesian mangrove forests. *Ecological Research* 14 (4): 409–413. <https://doi.org/10.1046/j.1440-1703.1999.00313.x>.
- Gerlach, M.J., S.E. Engelhart, A.C. Kemp, R.P. Moyer, J.M. Smoak, C.E. Bernhardt, and N. Cahill. 2017. Reconstructing Common Era relative sea-level change on the gulf coast of Florida. *Marine Geology* 390: 254–269. <https://doi.org/10.1016/j.margeo.2017.07.001>.
- Gonnea, M.E. 2016. Appendix D: Tampa Bay carbon burial rates across mangrove and salt marsh ecosystems. In: Sheehan L, Crooks S. Tampa Bay blue carbon assessment: summary of findings & addendum. Technical Reports #07–16 and #07a-16 of the Tampa Bay Estuary Program, St. Petersburg, FL. 50 pp. [http://www.tbep.tech.org/TBEP\\_TECH\\_PUBS/2016/TBEP\\_07\\_16\\_Tampa-Bay-Blue-Carbon-Assessment-Report-FINAL\\_June16-2016.pdf](http://www.tbep.tech.org/TBEP_TECH_PUBS/2016/TBEP_07_16_Tampa-Bay-Blue-Carbon-Assessment-Report-FINAL_June16-2016.pdf).
- Gress, S.K., M. Huxham, J.G. Kairo, L.M. Mugi, and R.A. Briers. 2017. Evaluating, predicting and mapping belowground carbon stores in Kenyan mangroves. *Global Change Biology* 23 (1): 224–234. <https://doi.org/10.1111/gcb.13438>.
- Han, X., L. Feng, C. Hu, and P. Kramer. 2018. Hurricane-induced changes in the Everglades National Park mangrove forest: Landsat observations between 1985 and 2017. *Journal of Geophysical Research: Biogeosciences* 123 (11): 3470–3488. <https://doi.org/10.1029/2018JG004501>.
- Hansen, M.C., P.V. Potapov, R. Moore, M. Hancher, S.A. Turubanova, A. Tyukavina, D. Thau, S.V. Stehman, S.J. Goetz, T.R. Loveland, and A. Kommareddy. 2013. High-resolution global maps of 21st-century forest cover change. *Science* 342 (6160): 850–853. <https://doi.org/10.1126/science.1244693>.
- Hengl, T., J. Mendes de Jesus, G.B. Heuvelink, M. Ruiperez Gonzalez, M. Kilibarda, A. Blagotić, W. Shangguan, M.N. Wright, X. Geng, B. Bauer-Marschallinger, and M.A. Guevara. 2017. SoilGrids250m: global gridded soil information based on machine learning. *PLoS one* 12 (2): e0169748. <https://doi.org/10.1371/journal.pone.0169748>.
- Henry, K.M., and R.R. Twilley. 2013. Soil development in a coastal Louisiana wetland during a climate-induced vegetation shift from salt marsh to mangrove. *Journal of Coastal Research* 29 (6): 1273–1283. <https://doi.org/10.2112/JCOASTRES-D-12-00184.1>.
- Hickey, S.M., N.J. Callow, S. Phinn, C.E. Lovelock, and C.M. Duarte. 2018. Spatial complexities in aboveground carbon stocks of a semi-arid mangrove community: A remote sensing height-biomass-carbon approach. *Estuarine, Coastal and Shelf Science* 200: 194–201.
- Hijmans, R.J. 2020. raster: geographic data analysis and modeling. R package version 3.0–12. <https://CRAN.R-project.org/package=raster>.
- Hladik, C., and M. Alber. 2012. Accuracy assessment and correction of a LIDAR-derived salt marsh digital elevation model. *Remote Sensing of Environment* 121: 224–235. <https://doi.org/10.1016/j.rse.2012.01.018>.
- Howard, J., S. Hoyt, K. Isensee, E. Pidgeon, and M. Telszewski, eds. 2014. Coastal blue carbon: methods for assessing carbon stocks and emissions factors in mangroves, tidal salt marshes, and seagrass meadows. Arlington: Conservation International, Intergovernmental Oceanographic Commission of UNESCO, International Union for Conservation of Nature.
- Hutchison, J., A. Manica, R. Swetnam, A. Balmford, and M. Spalding. 2014. Predicting global patterns in mangrove forest biomass. *Conservation Letters* 7 (3): 233–240. <https://doi.org/10.1111/conl.12060>.
- Jackson, K., G.R. Brooks, and R.A. Larson. 2021. Of marsh and mangrove: coupled biophysical and anthropogenic drivers of 20th century wetland conversion in Tampa Bay Estuary, Florida (USA). *Anthropocene* 34: 100295. <https://doi.org/10.1016/j.ancene.2021.100295>.
- Jardine, S.L., and J.V. Siikamäki. 2014. A global predictive model of carbon in mangrove soils. *Environmental Research Letters* 9 (10): 104013. <https://doi.org/10.1088/1748-9326/9/10/104013>.
- Jerath, M., M. Bhat, V.H. Rivera-Monroy, E. Castañeda-Moya, M. Simard, and R.R. Twilley. 2016. The role of economic, policy, and ecological factors in estimating the value of carbon stocks in Everglades mangrove forests, South Florida, USA. *Environmental Science & Policy* 66: 160–169. <https://www.sciencedirect.com/science/article/abs/pii/S1462901116306098>.
- Jones, M.C., G.L. Wingard, B. Stackhouse, K. Keller, D. Willard, M. Marot, B. Landacre, E. Bernhardt, and C. 2019. Rapid inundation of southern Florida coastline despite low relative sea-level rise rates during the late-Holocene. *Nature Communications* 10 (1): 1–13. <https://doi.org/10.1038/s41467-019-11138-4>.
- Kauffman, J.B., M.F. Adame, V.B. Arifanti, L.M. Schile-Beers, A.F. Bernardino, R.K. Bhomia, D.C. Donato, I.C. Feller, T.O. Ferreira, M.D.C. Jesus Garcia, and R.A. MacKenzie. 2020. Total ecosystem carbon stocks of mangroves across broad global environmental and physical gradients. *Ecological Monographs* 90 (2): e01405. <https://doi.org/10.1002/ecm.1405>.
- Kauffman, J.B., and D.C. Donato. 2012. Protocols for the measurement, monitoring and reporting of structure, biomass and carbon stocks in mangrove forests. Working paper 86. Bogor: Center for International Forestry Research.
- Kauffman, J.B., C. Heider, T.G. Cole, K.A. Dwire, and D.C. Donato. 2011. Ecosystem carbon stocks of Micronesian mangrove forests. *Wetlands* 31 (2): 343–352. <https://doi.org/10.1007/s13157-011-0148-9>.
- Khan, N.S., E. Ashe, B.P. Horton, A. Dutton, R.E. Kopp, G. Brocard, S.E. Engelhart, D.F. Hill, W.R. Peltier, C.H. Vane, and F.N. Scatena. 2017. Drivers of Holocene sea-level change in the Caribbean. *Quaternary Science Reviews* 155: 13–36. <https://doi.org/10.1016/j.quascirev.2016.08.032>.

- Khan, N.S., E. Ashe, R.P. Moyer, A.C. Kemp, S.E. Engelhart, M. Brain, L. Toth, A.R. Chappel, M. Christie, R. Kopp, and B.P. Horton. 2022. Relative sea-level change in South Florida during the past ~5 ka. *Global and Planetary Change* p.103902. <https://doi.org/10.1016/j.gloplacha.2022.103902>.
- Kottek, M., J. Grieser, C. Beck, B. Rudolf, and F. Rubel. 2006. World map of the Köppen–Geiger climate classification updated. *Meteorologische Zeitschrift* 15 (3): 259–263. <https://doi.org/10.5194/hess-11-1633-2007>.
- Krauss, K.W., A.W. Demopoulos, N. Cormier, A.S. From, J.P. McClain-Counts, and R.R. Lewis III. 2018. Ghost forests of Marco Island: Mangrove mortality driven by belowground soil structural shifts during tidal hydrologic alteration. *Estuarine, Coastal and Shelf Science* 212: 51–62. <https://doi.org/10.1016/j.ecss.2018.06.026>.
- Krauss, K.W., A.S. From, T.W. Doyle, T.J. Doyle, and M.J. Barry. 2011. Sea-level rise and landscape change influence mangrove encroachment onto marsh in the Ten Thousand Islands region of Florida, USA. *Journal of Coastal Conservation* 15 (4): 629–638. <https://doi.org/10.1007/s11852-011-0153-4>.
- Kulawardhana, R.W., S.C. Popescu, and R.A. Feagin. 2014. Fusion of lidar and multispectral data to quantify salt marsh carbon stocks. *Remote Sensing of Environment* 154: 345–357. <https://doi.org/10.1016/j.rse.2013.10.036>.
- Lagomasino, D., T. Fatoyinbo, E. Castañeda-Moya, B.D. Cook, P.M. Montesano, C.S. Neigh, L.A. Corp, L.E. Ott, S. Chavez, and D.C. Morton. 2021. Storm surge and ponding explain mangrove dieback in southwest Florida following Hurricane Irma. *Nature Communications* 12 (1): 1–8. <https://doi.org/10.1038/s41467-021-24253-y>.
- Lara, R.J., and M.C. Cohen. 2006. Sediment porewater salinity, inundation frequency and mangrove vegetation height in Bragança, North Brazil: An ecohydrology-based empirical model. *Wetlands Ecology and Management* 14 (4): 349–358. <https://doi.org/10.1007/s11273-005-4991-4>.
- Leblanc, M., J. Lemoalle, J.C. Bader, S. Tweed, and L. Mofor. 2011. Thermal remote sensing of water under flooded vegetation: New observations of inundation patterns for the ‘Small’ Lake Chad. *Journal of Hydrology* 404 (1–2): 87–98. <https://doi.org/10.1016/j.jhydrol.2011.04.023>.
- Lewis III, R.R., E.C. Milbrandt, B. Brown, K.W. Krauss, A.S. Rovai, J.W. Beaver, and L.L. Flynn. 2016. Stress in mangrove forests: Early detection and preemptive rehabilitation are essential for future successful worldwide mangrove forest management. *Marine Pollution Bulletin* 109: 764–771. <https://doi.org/10.1016/j.marpolbul.2016.03.006>.
- Liaw, A., and M. Wiener. 2002. Classification and Regression by randomForest. *R News* 2 (3): 18–22.
- Liu, H., H. Ren, D. Hui, W. Wang, B. Liao, and Q. Cao. 2014. Carbon stocks and potential carbon storage in the mangrove forests of China. *Journal of Environmental Management* 133: 86–93. <https://doi.org/10.1016/j.jenvman.2013.11.037>.
- Lu, D., Q. Chen, G. Wang, L. Liu, G. Li, and E. Moran. 2016. A survey of remote sensing-based aboveground biomass estimation methods in forest ecosystems. *International Journal of Digital Earth* 9 (1): 63–105. <https://doi.org/10.1080/17538947.2014.990526>.
- Lugo, A.E., and S.C. Snedaker. 1974. The ecology of mangroves. *Annual Review of Ecology and Systematics* 5 (1): 39–64.
- Lynch, J.C. 1989. Sedimentation and nutrient accumulation in mangrove ecosystems of the Gulf of Mexico. M.S. Thesis, The University of Southwestern Louisiana. Lafayette, LA.
- Macreadie, P.I., A. Anton, J.A. Raven, N. Beaumont, R.M. Connolly, D.A. Friess, J.J. Kelleway, H. Kennedy, T. Kuwae, P.S. Lavery, and C.E. Lovelock. 2019. The future of Blue Carbon science. *Nature Communications* 10 (1): 1–13. <https://doi.org/10.1038/s41467-019-11693-w>.
- Macy, A., M.J. Osland, J.A. Cherry, and J. Cebrian. 2021. Changes in ecosystem nitrogen and carbon allocation with black mangrove (*Avicennia germinans*) encroachment into *Spartina alterniflora* salt marsh. *Ecosystems* 24 (5): 1007–1023. <https://doi.org/10.1007/s10021-020-00565-w>.
- Mahdavi, S., B. Salehi, J. Granger, M. Amani, B. Brisco, and W. Huang. 2018. Remote sensing for wetland classification: A comprehensive review. *Giscience & Remote Sensing* 55 (5): 623–658. <https://doi.org/10.1080/15481603.2017.1419602>.
- Maher, D.T., I.R. Santos, L. Golsby-Smith, J. Gleeson, and B.D. Eyre. 2013. Groundwater-derived dissolved inorganic and organic carbon exports from a mangrove tidal creek: The missing mangrove carbon sink? *Limnology and Oceanography* 58 (2): 475–488. <https://doi.org/10.4319/lo.2013.58.2.0475>.
- Marchio, D.A., M. Savarese, B. Bovard, and W.J. Mitsch. 2016. Carbon sequestration and sedimentation in mangrove swamps influenced by hydrogeomorphic conditions and urbanization in Southwest Florida. *Forests* 7 (6): 116. <https://doi.org/10.3390/f7060116>.
- McCarthy, M.J., B. Jessen, M.J. Barry, M. Figueroa, J. McIntosh, T. Murray, J. Schmid, and F.E. Muller-Karger. 2020. Automated high-resolution time series mapping of mangrove forests damaged by Hurricane Irma in Southwest Florida. *Remote Sensing* 12 (11): 1740. <https://doi.org/10.3390/rs12111740>.
- McKee, K.L. 2011. Biophysical controls on accretion and elevation change in Caribbean mangrove ecosystems. *Estuarine and Coastal Shelf Science* 91: 475–483. <https://doi.org/10.1016/j.ecss.2010.05.001>.
- Medeiros, S., S. Hagen, J. Weishampel, and J. Angelo. 2015. Adjusting lidar-derived digital terrain models in coastal marshes based on estimated aboveground biomass density. *Remote Sensing* 7 (4): 3507–3525. <https://doi.org/10.3390/rs70403507>.
- Middleton, B.A., and K.L. McKee. 2001. Degradation of mangrove tissues and implications for peat formation in Belizean island forests. *Journal of Ecology* 89 (5): 818–828. <https://www.jstor.org/stable/3072155>.
- Navarro, A., M. Young, B. Allan, P. Carnell, P. Macreadie, and D. Ierodiakonou. 2020. The application of unmanned aerial vehicles (UAVs) to estimate above-ground biomass of mangrove ecosystems. *Remote Sensing of Environment* 242:111747. <https://doi.org/10.1016/j.rse.2020.111747>.
- Orson, R.A., R.S. Warren, and W.A. Niering. 1987. Development of a tidal marsh in a New England river valley. *Estuaries* 10 (1): 20–27. <https://doi.org/10.2307/1352021>.
- Osland, M.J., L.C. Feher, G.H. Anderson, W.C. Vervaek, K.W. Krauss, K.R. Whelan, K.M. Balentine, G. Tiling-Range, T.J. Smith, and D.R. Cahoon. 2020. A tropical cyclone-induced ecological regime shift: Mangrove forest conversion to mudflat in Everglades National Park (Florida, USA). *Wetlands* 40 (5): 1445–1458. <https://doi.org/10.1007/s13157-020-01291-8>.
- Osland, M.J., J.B. Grace, C.L. Stagg, R.H. Day, S.B. Hartley, N.M. Enwright, and C.A. Gabler. 2016. U.S. Gulf of Mexico coast (TX, MS, AL, and FL) Vegetation, soil, and landscape data (2013–2014): U.S. *Geological Survey Data Release*. <https://doi.org/10.5066/F7J1017G>.
- Osland, M.J., A.R. Hughes, A.R. Armitage, S.B. Scyphers, J. Cebrian, S.H. Swinea, C.C. Shepard, M.S. Allen, L.C. Feher, J.A. Nelson, and C.L. O’Brien. 2022. The impacts of mangrove range expansion on wetland ecosystem services in the southeastern United States: current understanding, knowledge gaps, and emerging research needs. *Global Change Biology* 28(10): 3163–3187. <https://doi.org/10.1111/gcb.16111>
- Osland, M.J., A.C. Spivak, J.A. Nestlerode, J.M. Lessmann, A.E. Almario, P.T. Heitmuller, M.J. Russell, K.W. Krauss, F. Alvarez, D.D. Dantin, and J.E. Harvey. 2012. Ecosystem development after mangrove wetland creation: Plant–soil change across a 20-year

- chronosequence. *Ecosystems* 15 (5): 848–866. <https://doi.org/10.1007/s10021-012-9551-1>.
- Ouyang, X., S.Y. Lee, and R.M. Connolly. 2017. Structural equation modelling reveals factors regulating surface sediment organic carbon content and CO<sub>2</sub> efflux in a subtropical mangrove. *Science of the Total Environment* 578: 513–522. <https://doi.org/10.1016/j.scitotenv.2016.10.218>.
- Paolini, J.E., and L.E. Sánchez-Arias. 2008. Comparative biochemical study of the rhizosphere of *Rhizophora mangle* and its associated species *Cyperus* sp. in the Ciénaga de Soledad (Colombia). In *Mangroves and halophytes: Restoration and Utilisation* (pp. 79–84). Springer, Dordrecht. [https://doi.org/10.1007/978-1-4020-6720-4\\_8](https://doi.org/10.1007/978-1-4020-6720-4_8).
- Patil, V., A. Singh, N. Naik, and S. Unnikrishnan. 2015. Estimation of mangrove carbon stocks by applying remote sensing and GIS techniques. *Wetlands* 35 (4): 695–707. <https://doi.org/10.1007/s13157-015-0660-4>.
- Peneva-Reed, E.I., K.W. Krauss, E.L. Bullock, Z. Zhu, V.L. Woltz, J.Z. Drexler, J.R. Conrad, and S.V. Stehman. 2021. Carbon stock losses and recovery observed for a mangrove ecosystem following a major hurricane in Southwest Florida. *Estuarine, Coastal and Shelf Science* 248: 106750. <https://doi.org/10.1016/j.ecss.2020.106750>.
- Peneva-Reed, E.I., and Z. Zhu. 2019. Mangrove Data Collected from J.N. "Ding" Darling National Wildlife Refuge, Sanibel Island, Florida, United States: U.S. Geological Survey data release. <https://doi.org/10.5066/P9P2PHU3>.
- Plater, A.J., J.R. Kirby, J.F. Boyle, T. Shaw, and H. Mills. 2015. Loss on ignition and organic content. In *Handbook of Sea-Level Research*, eds. I. Shennan, A.J. Long, and B.P. Horton, 312–330. New York: J. Wiley and Sons Ltd. <https://doi.org/10.1002/9781118452547.ch21>.
- QGIS Development Team. 2020. QGIS Geographic Information System. Open Source Geospatial Foundation Project. <https://qgis.org/en/site/>.
- R Core Team. 2019. R: A language and environment for statistical computing. R Foundation for Statistical Computing, Vienna, Austria. <https://www.R-project.org/>.
- Raabe, E.A., L.C. Roy, and C.C. McIvor. 2012. Tampa Bay coastal wetlands: Nineteenth to twentieth century tidal marsh-to-mangrove conversion. *Estuaries and Coasts* 35 (5): 1145–1162. <https://doi.org/10.1007/s12237-012-9503-1>.
- Radabaugh, K.R., E.E. Dontis, A.R. Chappel, C.E. Russo, and R.P. Moyer. 2021. Early indicators of stress in mangrove forests with altered hydrology in Tampa Bay, Florida, USA. *Estuarine, Coastal and Shelf Science* 254: 107324. <https://doi.org/10.1016/j.ecss.2021.107324>.
- Radabaugh, K.R., R.P. Moyer, A.R. Chappel, E.E. Dontis, C.E. Russo, K.M. Joyse, M.W. Bownik, A.H. Goeckner, and N.S. Khan. 2020. Mangrove damage, delayed mortality, and early recovery following Hurricane Irma at two landfall sites in southwest Florida, USA. *Estuaries and Coasts* 43: 1104–1118. <https://doi.org/10.1007/s12237-019-00564-8>.
- Radabaugh, K.R., R.P. Moyer, A.R. Chappel, C.E. Powell, I. Bociu, B.C. Clark, and J.M. Smoak. 2018. Coastal blue carbon assessment of mangroves, salt marshes, and salt barrens in Tampa Bay, Florida, USA. *Estuaries and Coasts* 41 (5): 1496–1510. <https://doi.org/10.1007/s12237-017-0362-7>.
- Radabaugh, K.R., C.E. Powell, I. Bociu, B.C. Clark, and R.P. Moyer. 2017. Plant size metrics and organic carbon content of Florida salt marsh vegetation. *Wetlands Ecology and Management* 25 (4): 443–455. <https://doi.org/10.1007/s11273-016-9527-6>.
- Rogers, J.N., C.E. Parrish, L.G. Ward, and D.M. Burdick. 2015. Evaluation of field-measured vertical obscuration and full waveform lidar to assess salt marsh vegetation biophysical parameters. *Remote Sensing of Environment* 156: 264–275. <https://doi.org/10.1016/j.rse.2014.09.035>.
- Roner, M., A. D'Alpaos, M. Ghinassi, M. Marani, S. Silvestri, E. Franceschinis, and N. Realdon. 2016. Spatial variation of salt-marsh organic and inorganic deposition and organic carbon accumulation: Inferences from the Venice lagoon, Italy. *Advances in Water Resources* 93: 276–287. <https://doi.org/10.1016/j.advwatres.2015.11.011>.
- Rovai, A.S., R.R. Twilley, E. Castañeda-Moya, P. Riul, M. Cifuentes-Jara, M. Manrow-Villalobos, P.A. Horta, J.C. Simonassi, A.L. Fonseca, and P.R. Pagliosa. 2018. Global controls on carbon storage in mangrove soils. *Nature Climate Change* 8 (6): 534–538. <https://doi.org/10.1038/s41558-018-0162-5>.
- Saintilan, N., N.S. Khan, E. Ashe, J.J. Kelleway, K. Rogers, C.D. Woodroffe, and B.P. Horton. 2020. Thresholds of mangrove survival under rapid sea level rise. *Science* 368 (6495): 1118–1121. <https://doi.org/10.1126/science.aba2656>.
- Saintilan, N., K. Rogers, D. Mazumder, and C. Woodroffe. 2013. Allochthonous and autochthonous contributions to carbon accumulation and carbon store in southeastern Australian coastal wetlands. *Estuarine, Coastal and Shelf Science* 128: 84–92. <https://doi.org/10.1016/j.ecss.2013.05.010>.
- Sanderman, J., T. Hengl, G. Fiske, K. Solvik, M.F. Adame, L. Benson, J.J. Bukoski, P. Carnell, M. Cifuentes-Jara, D. Donato, and C. Duncan. 2018. A global map of mangrove forest soil carbon at 30 m spatial resolution. *Environmental Research Letters* 13 (5): 055002. <https://doi.org/10.1088/1748-9326/aabe1c>.
- Sanders, C.J., D.T. Maher, D.R. Tait, D. Williams, C. Holloway, J.Z. Sippo, and I.R. Santos. 2016. Are global mangrove carbon stocks driven by rainfall? *Journal of Geophysical Research: Biogeosciences* 121 (10): 2600–2609. <https://doi.org/10.1002/2016JG003510>.
- Saravanan, S., R. Jegankumar, A. Selvaraj, J.J. Jennifer, and K.S.S. Parthasarathy. 2019. Utility of landsat data for assessing mangrove degradation in Muthupet Lagoon, South India. In *Coastal Zone Management*. 471–484. Elsevier. <https://doi.org/10.1016/B978-0-12-814350-6.00020-3>.
- Schafer, C. 2020. Mechanisms of carbon movement and stabilization in mangrove wetlands. M.S. Thesis, University of South Florida, College of Marine Science, Tampa, FL.
- SFWMD (South Florida Water Management District). 2018. Land cover land use 2014–2016. <https://sfwmd.maps.arcgis.com/home/item.html?id=266a64a897514090842e283311c12d30>.
- Shi, T., J. Liu, Z. Hu, H. Liu, J. Wang, and G. Wu. 2016. New spectral metrics for mangrove forest identification. *Remote Sensing Letters* 7 (9): 885–894. <https://doi.org/10.1080/2150704X.2016.1195935>.
- Simard, M., L. Fatoyinbo, C. Smetanka, V.H. Rivera-Monroy, E. Castañeda-Moya, N. Thomas, and T. Van der Stocken. 2019a. Mangrove canopy height globally related to precipitation, temperature and cyclone frequency. *Nature Geoscience* 12 (1): 40–45. <https://doi.org/10.1038/s41561-018-0279-1>.
- Simard, M., T. Fatoyinbo, C. Smetanka, V.H. Rivera-Monroy, E. Castañeda-Moya, N. Thomas, and Van der stocken, T. 2019b. Global mangrove distribution, aboveground biomass, and canopy height. ORNL DAAC, Oak Ridge, Tennessee, USA. <https://doi.org/10.3334/ORN LDAAC/1665>.
- Simard, M., K. Zhang, V.H. Rivera-Monroy, M.S. Ross, P.L. Ruiz, E. Castañeda-Moya, R.R. Twilley, and E. Rodriguez. 2006. Mapping height and biomass of mangrove forests in Everglades National Park with SRTM elevation data. *Photogrammetric Engineering & Remote Sensing* 72 (3): 299–311. <https://doi.org/10.14358/PERS.72.3.299>.
- Simpson, L.T., C.M. Stein, T.Z. Osborne, and I.C. Feller. 2019. Mangroves dramatically increase carbon storage after 3 years of

- encroachment. *Hydrobiologia* 834 (1): 13–26. <https://doi.org/10.1007/s10750-019-3905-z>.
- Smith, T.J. 1993. Forest structure. *Coastal and Estuarine Studies: Tropical Mangrove Ecosystems* 41: 101–136.
- Smith, T.J., G.H. Anderson, K. Balentine, G. Tiling, G.A. Ward, and K.R. Whelan. 2009. Cumulative impacts of hurricanes on Florida mangrove ecosystems: Sediment deposition, storm surges and vegetation. *Wetlands* 29 (1): 24–34. <https://doi.org/10.1672/08-40.1>.
- Smoak, J.M., J.L. Breithaupt, T.J. Smith III., and C.J. Sanders. 2013. Sediment accretion and organic carbon burial relative to sea-level rise and storm events in two mangrove forests in Everglades National Park. *CATENA* 104: 58–66. <https://doi.org/10.1016/j.catena.2012.10.009>.
- Steinmuller, H.E., J.L. Breithaupt, K.E. Engelbert, P. Assavanuvat, and T.S. Bianchi. 2022. Coastal wetland soil carbon storage at mangrove range limits in Apalachicola Bay, FL: Observations and expectations. *Frontiers in Forests and Global Change* 5: 852910. <https://doi.org/10.3389/ffgc.2022.852910>.
- Stovall, A.E., T. Fatoyinbo, N.M. Thomas, J. Armston, M.O. Ebanega, M. Simard, C. Trettin, R.V.O. Zogo, I.A. Aken, M. Debina, and A.M.M. Kemoe. 2021. Comprehensive comparison of airborne and spaceborne SAR and LiDAR estimates of forest structure in the tallest mangrove forest on earth. *Science of Remote Sensing* 4: 100034. <https://doi.org/10.1016/j.srs.2021.100034>.
- Stringer, C.E., C.C. Trettin, S.J. Zarnoch, and W. Tang. 2015. Carbon stocks of mangroves within the Zambezi River Delta, Mozambique. *Forest Ecology and Management* 354: 139–148. <https://doi.org/10.1016/j.foreco.2015.06.027>.
- SWFWMD (Southwest Florida Water Management District). 2019. Southwest Florida Water Management District Land Use Land Cover 2017.
- Thomas, N., M. Simard, E. Castañeda-Moya, K. Byrd, L. Windham-Myers, A. Bevington, and R.R. Twilley. 2019. High-resolution mapping of biomass and distribution of marsh and forested wetlands in southeastern coastal Louisiana. *International Journal of Applied Earth Observation and Geoinformation* 80: 257–267.
- Thu, P.M., and J. Populus. 2007. Status and changes of mangrove forest in Mekong Delta: Case study in Tra Vinh. *Vietnam. Estuarine, Coastal and Shelf Science* 71 (1–2): 98–109. <https://doi.org/10.1016/j.ecss.2006.08.007>.
- Toscano, M.A., J.L. Gonzalez, and K.R. Whelan. 2018. Calibrated density profiles of Caribbean mangrove peat sequences from computed tomography for assessment of peat preservation, compaction, and impacts on sea-level reconstructions. *Quaternary Research* 89 (1): 201–222. <https://doi.org/10.1017/qua.2017.101>.
- U.S. Geological Survey. 2019. 3D Elevation Program (3DEP) seamless product. U.S. Geological Survey. <https://apps.nationalmap.gov/downloader/#/productGroupSearch>.
- Valderrama-Landeros, L., F. Flores-de-Santiago, J.M. Kovacs, and F. Flores-Verdugo. 2018. An assessment of commonly employed satellite-based remote sensors for mapping mangrove species in Mexico using an NDVI-based classification scheme. *Environmental Monitoring and Assessment* 190 (1): 1–13. <https://doi.org/10.1007/s10661-017-6399-z>.
- Wang, D., B. Wan, P. Qiu, Y. Su, Q. Guo, R. Wang, F. Sun, and X. Wu. 2018. Evaluating the performance of Sentinel-2, Landsat 8 and Pleiades-1 in mapping mangrove extent and species. *Remote Sensing* 10 (9): 1468. <https://doi.org/10.3390/rs10091468>.
- Wang, J., Z. Liu, H. Yu, and F. Li. 2017. Mapping *Spartina alterniflora* biomass using Lidar and hyperspectral data. *Remote Sensing* 9 (6): 589. <https://doi.org/10.3390/rs9060589>.
- Whelan, K.R.T. 2005. The successional dynamics of lightning-initiated canopy gaps in the mangrove forests of Shark River, Everglades National Park, USA. PhD Dissertation, Florida International University.
- White, E., and D. Kaplan. 2017. Restore or retreat? Saltwater intrusion and water management in coastal wetlands. *Ecosystem Health and Sustainability* 3 (1): e01258. <https://doi.org/10.1002/ehs2.1258>.
- Wicaksono, P. 2017. Mangrove above-ground carbon stock mapping of multi-resolution passive remote-sensing systems. *International Journal of Remote Sensing* 38 (6): 1551–1578. <https://doi.org/10.1080/01431161.2017.1283072>.
- Wilson, B.J., S. Servais, S.P. Charles, S.E. Davis, E.E. Gaiser, J.S. Kominoski, J.H. Richards, and T.G. Troxler. 2018. Declines in plant productivity drive carbon loss from brackish coastal wetland mesocosms exposed to saltwater intrusion. *Estuaries and Coasts* 41 (8): 2147–2158. <https://doi.org/10.1007/s12237-018-0438-z>.
- Winarso, G., Y. Vetrira, A.D. Purwanto, N. Anggraini, S. Darmawan, and D.M. Yuwono. 2017. Mangrove above ground biomass estimation using combination of Landsat 8 and ALOS PALSAR data. *International Journal of Remote Sensing and Earth Sciences (IJReSES)* 12 (2): 85–96. <https://doi.org/10.30536/ij.ijreses.2015.v12.a2687>.
- Worthington, T.A., P.S. Zu Ermgassen, D.A. Friess, K.W. Krauss, C.E. Lovelock, J. Thorley, R. Tingey, C.D. Woodroffe, P. Bunting, N. Cormier, and D. Lagomasino. 2020. A global biophysical typology of mangroves and its relevance for ecosystem structure and deforestation. *Scientific Reports* 10 (1): 1–11. <https://doi.org/10.1038/s41598-020-71194-5>.
- Zhang, K., B. Thapa, M. Ross, and D. Gann. 2016. Remote sensing of seasonal changes and disturbances in mangrove forest: a case study from South Florida. *Ecosphere* 7 (6): e01366. <https://doi.org/10.1002/ecs2.1366>.

Springer Nature or its licensor (e.g. a society or other partner) holds exclusive rights to this article under a publishing agreement with the author(s) or other rightsholder(s); author self-archiving of the accepted manuscript version of this article is solely governed by the terms of such publishing agreement and applicable law.